Supplementary Information (SI) for Journal of Materials Chemistry B.

Understanding selective sensing of human serum albumin using a D-π-A probe: A Photophysical and Computational Approach

Anamika Bandyopadhyay and Anupam Bhattacharya

Department of Chemistry, Birla Institute of Technology and Science-Pilani (Hyderabad Campus), Hyderabad-500078, India.

E-mail: anupam@hyderabad.bits-pilani.ac.in; Tel: +91-40-66303522.

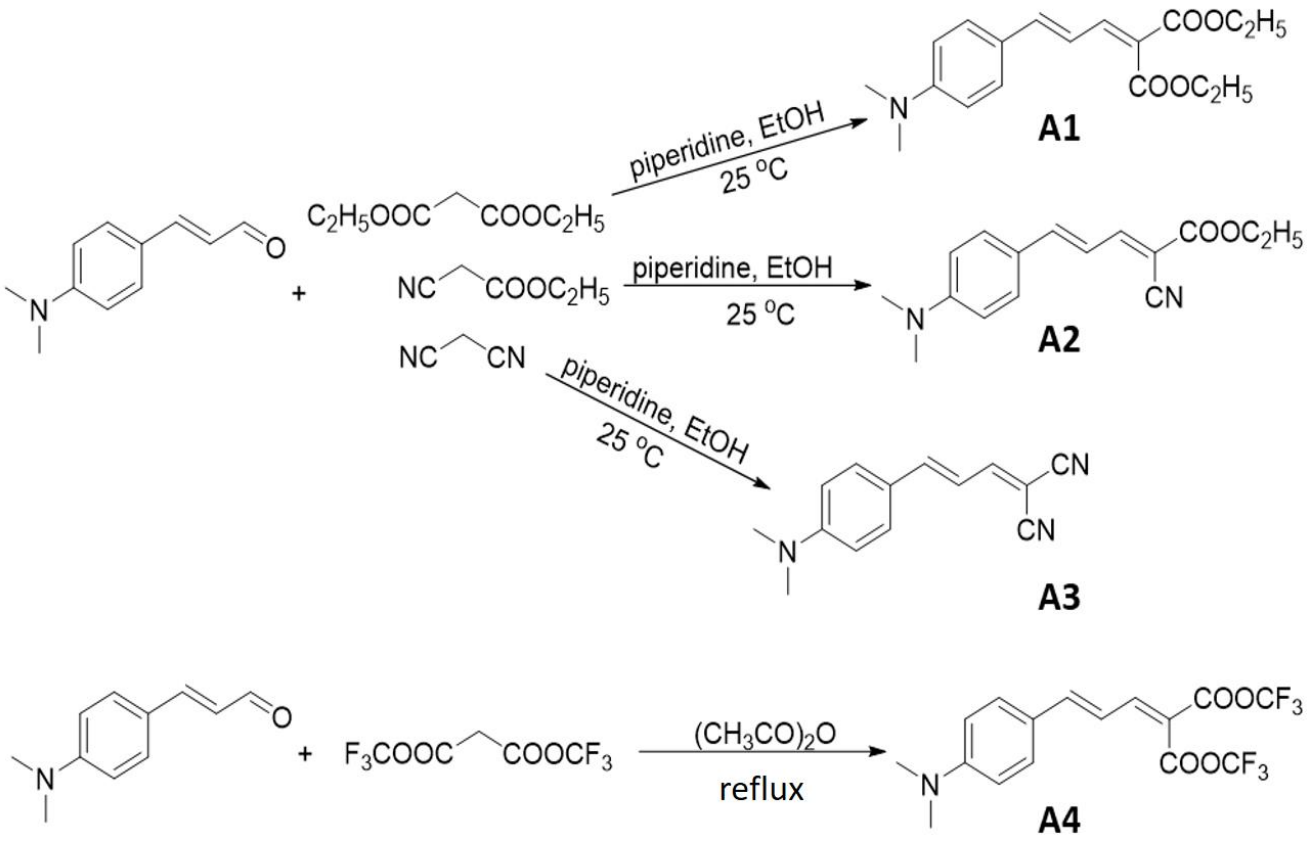

Figure S1: Synthetic scheme

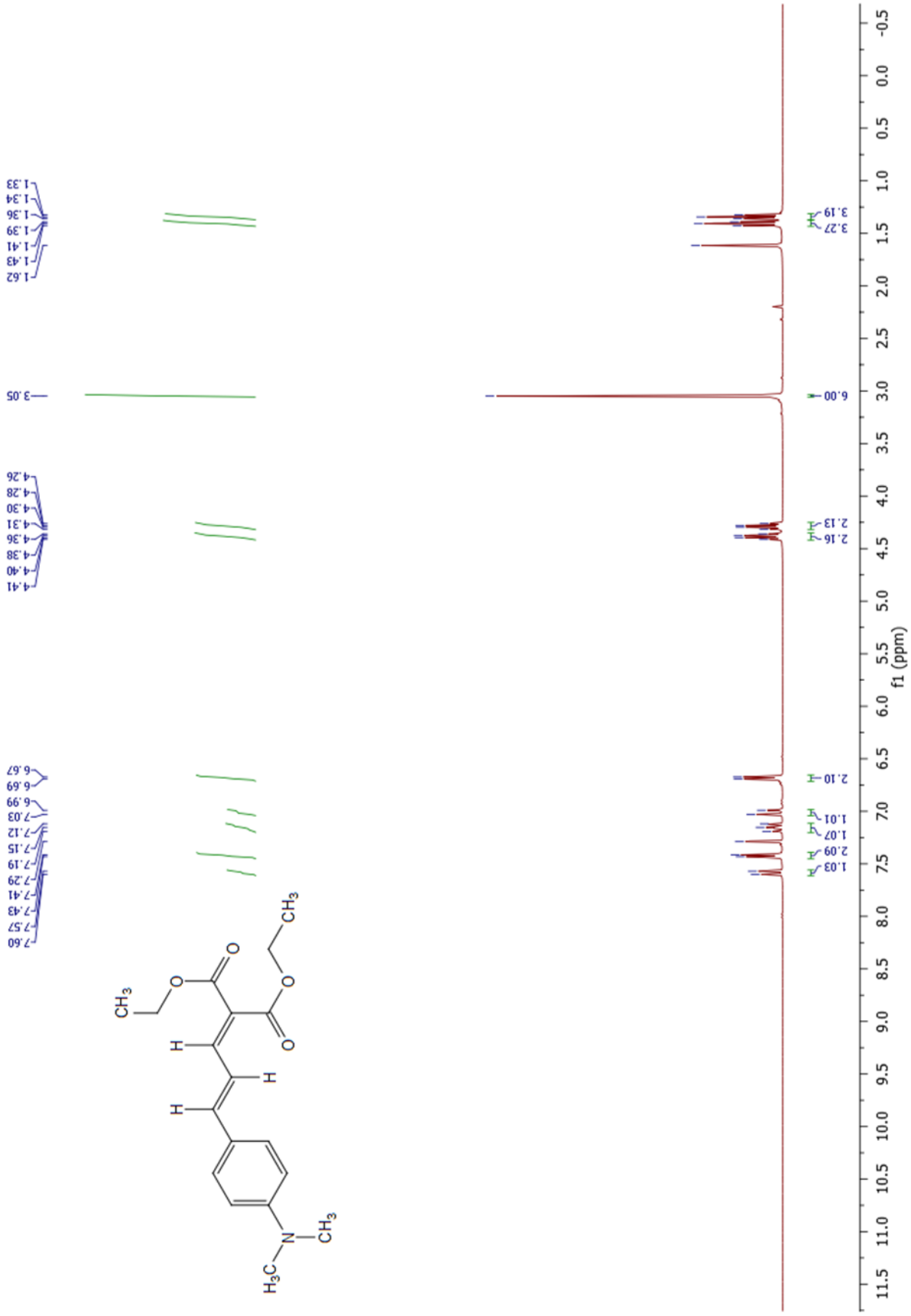

Figure S2: ^{1}H NMR spectrum of **A1** in $CDCl_3$.

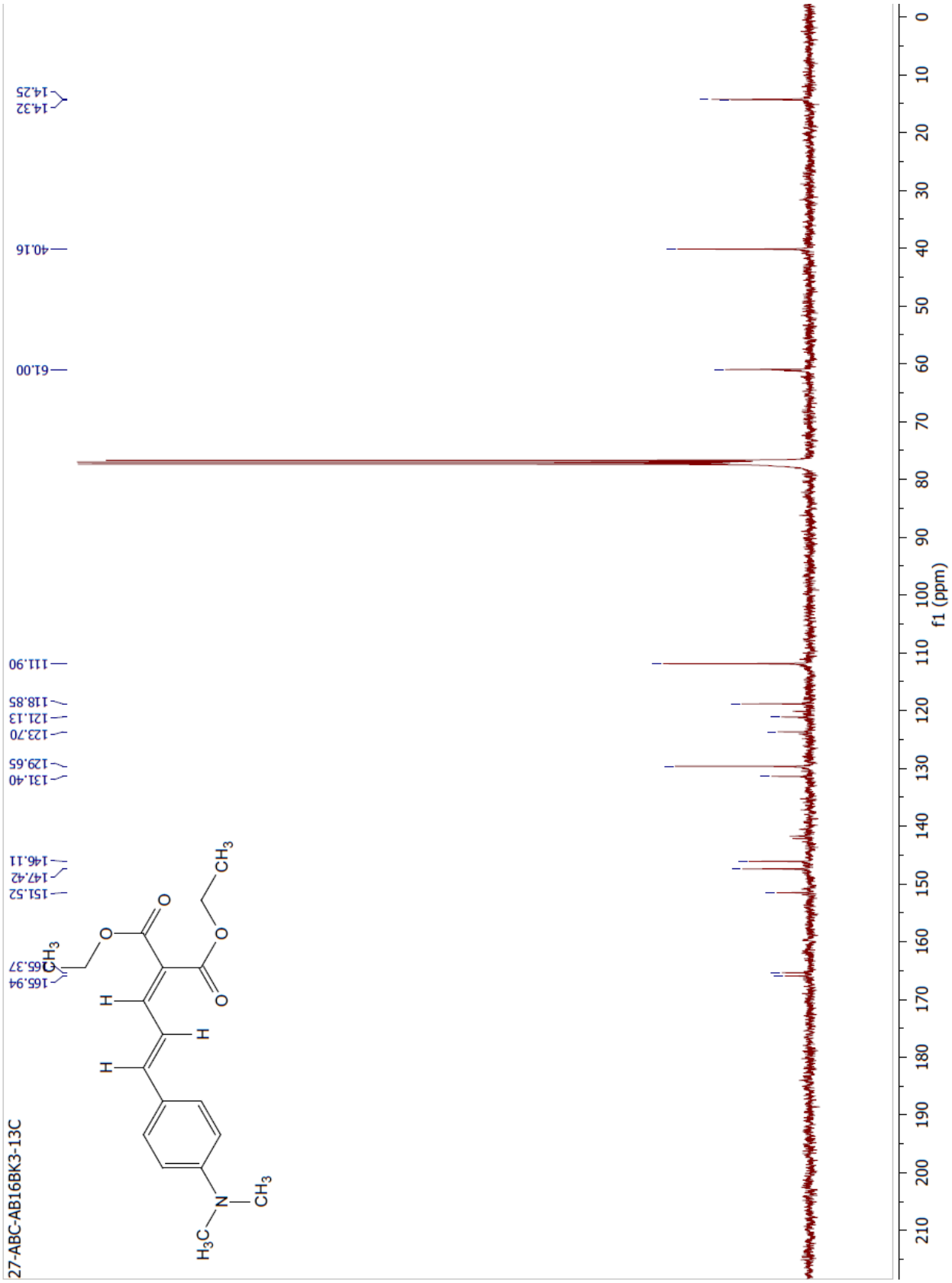

Figure S3: ^{13}C NMR spectrum of **A1** in $CDCl_3$.

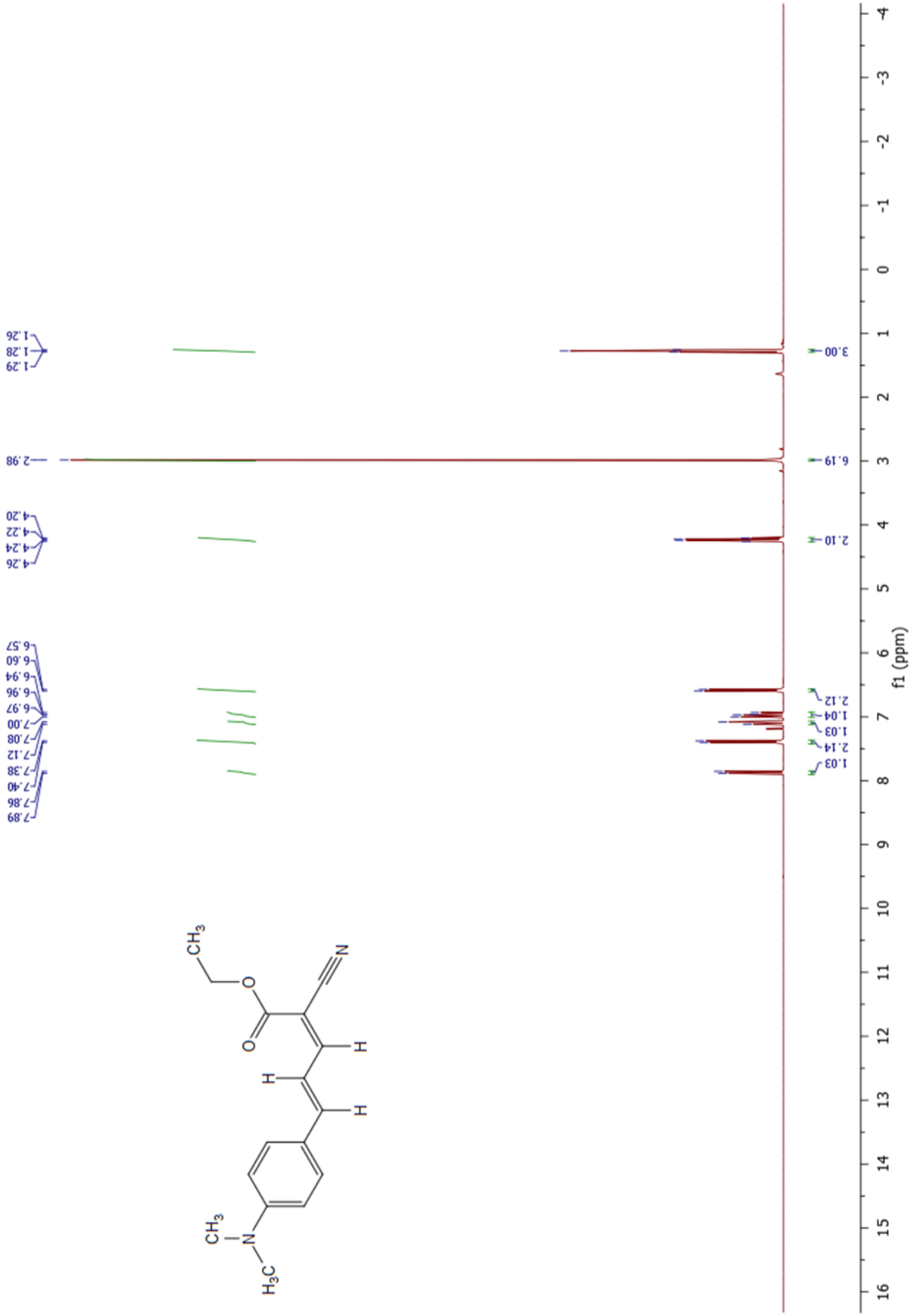

Figure S4: ^{1}H NMR spectrum of **A2** in $CDCl_3$.

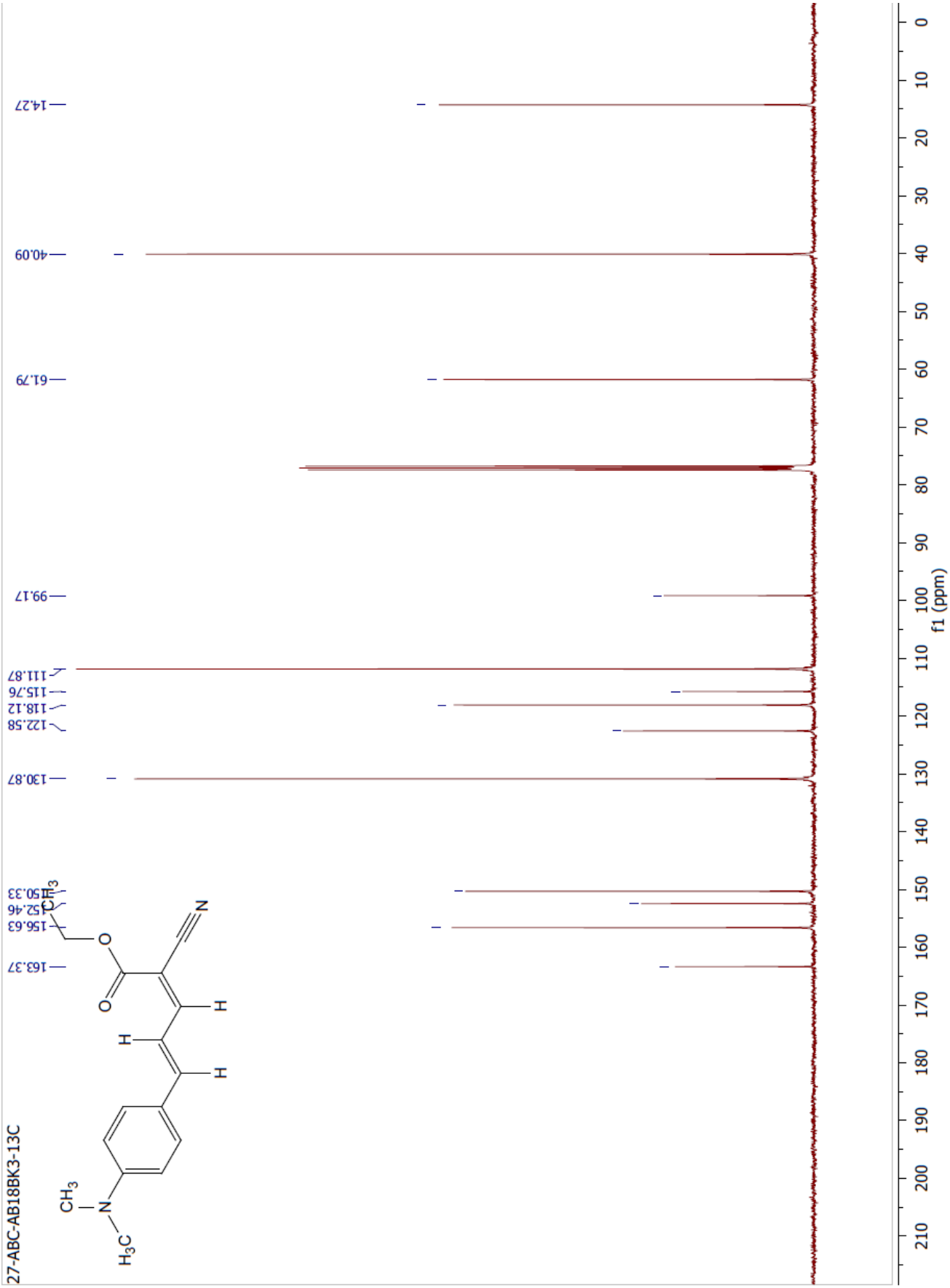

Figure S5: ^{13}C NMR spectrum of **A2** in $CDCl_3$.

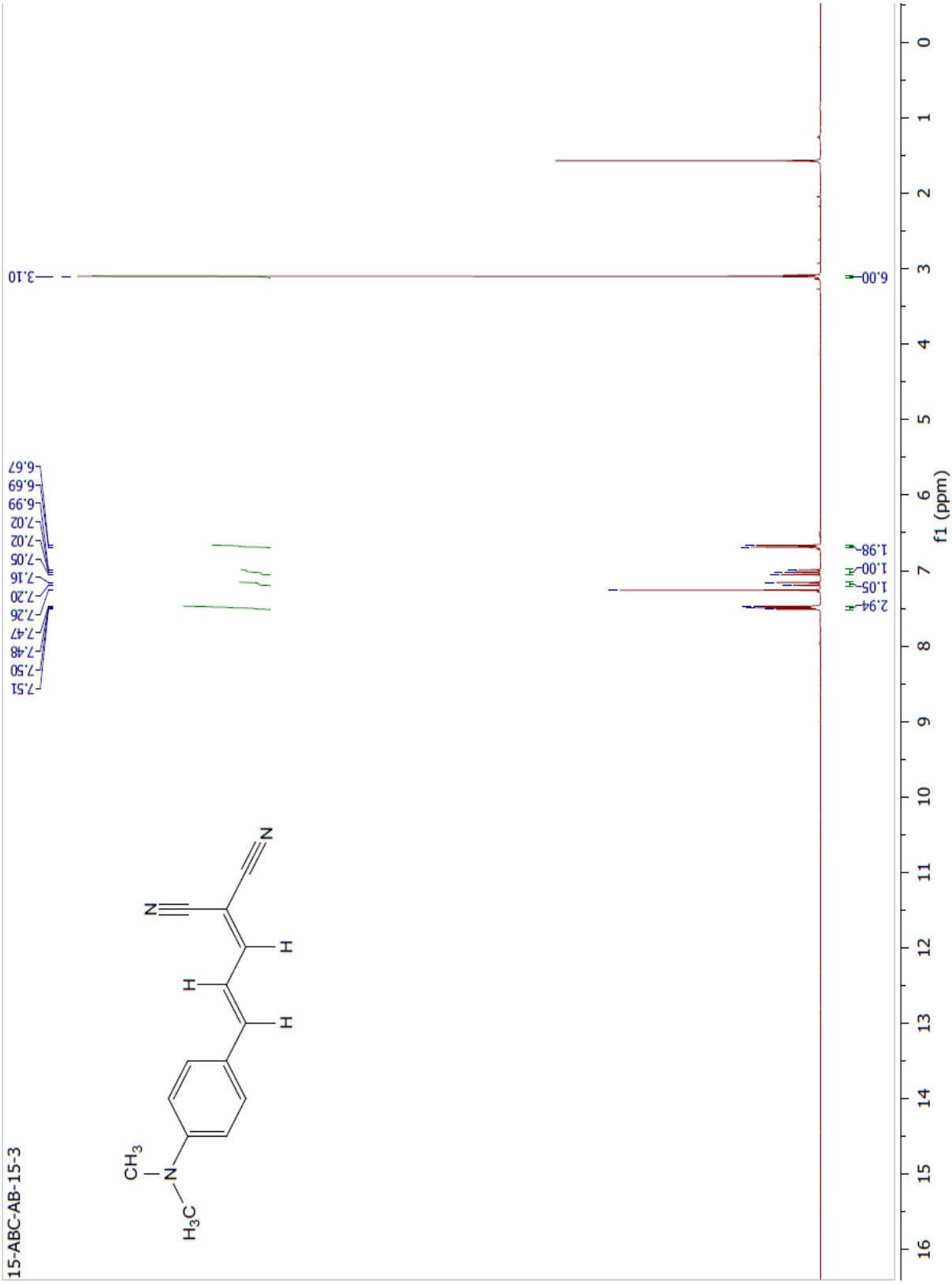

Figure S6: ^{1}H NMR spectrum of **A3** in $CDCl_3$.

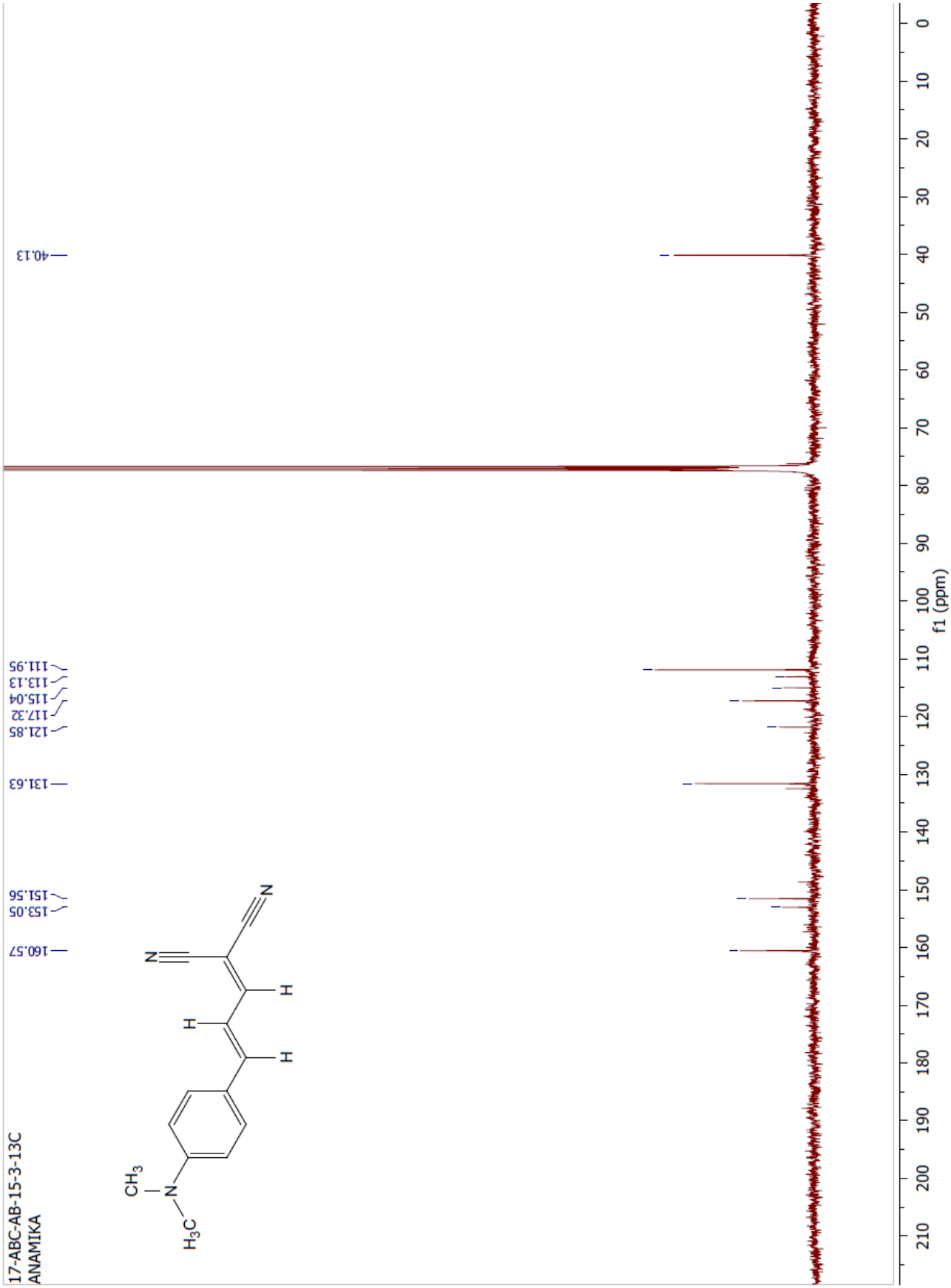

Figure S7: ^{13}C NMR spectrum of **A3** in $CDCl_3$.

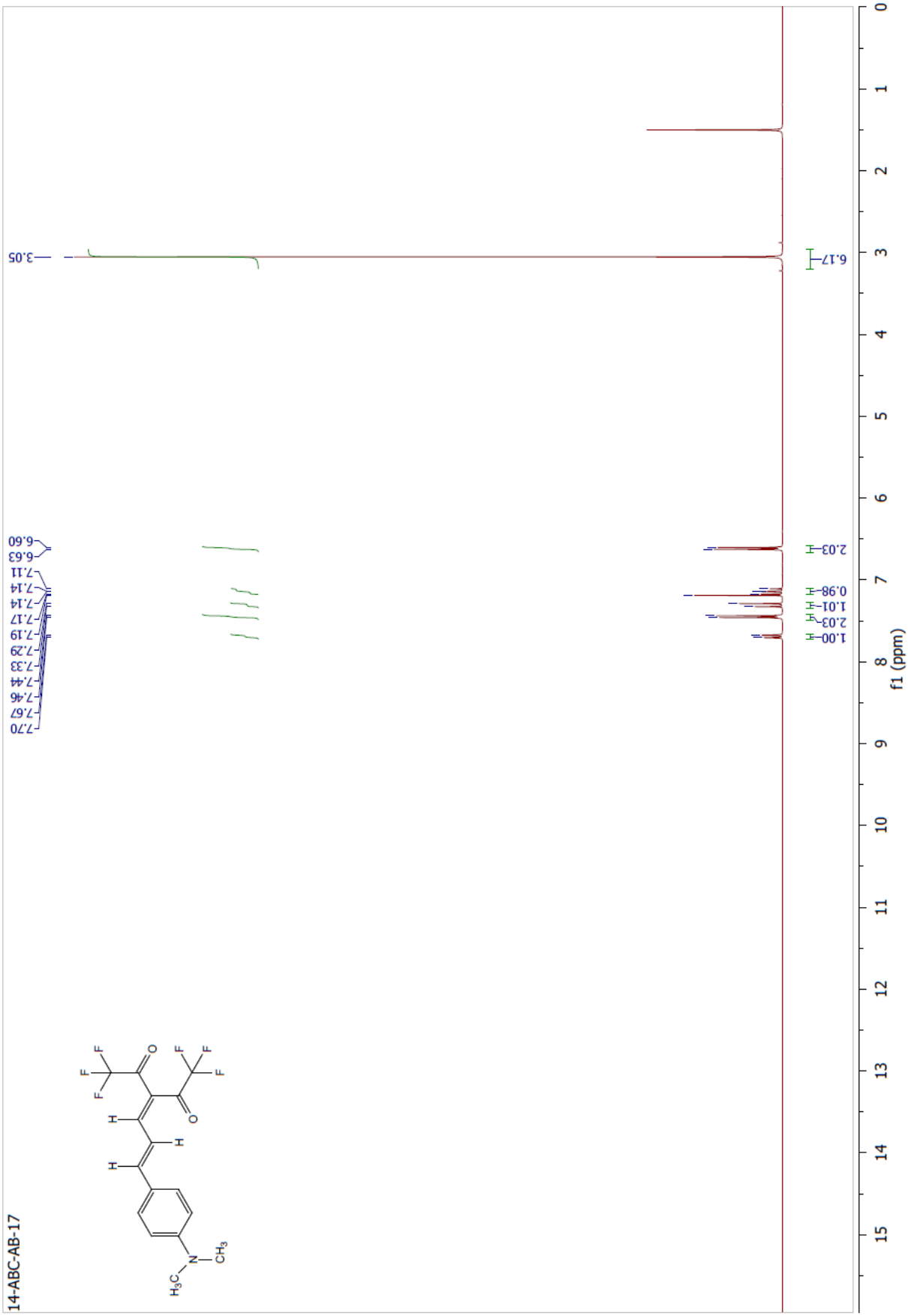

Figure S8: ^{1}H NMR spectrum of **A4** in $CDCl_3$.

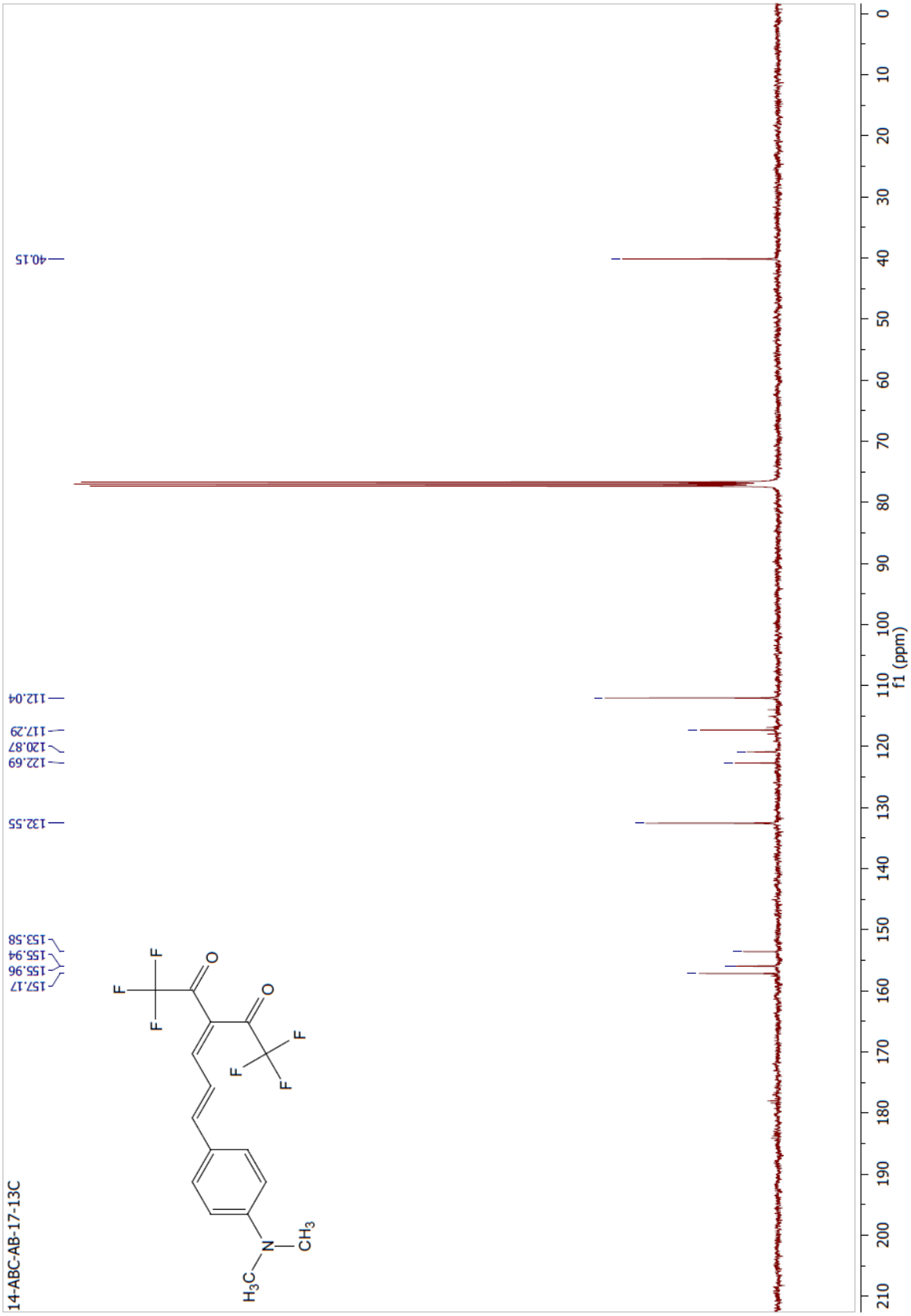

Figure S9: ^{13}C NMR spectrum of **A4** in $CDCl_3$.

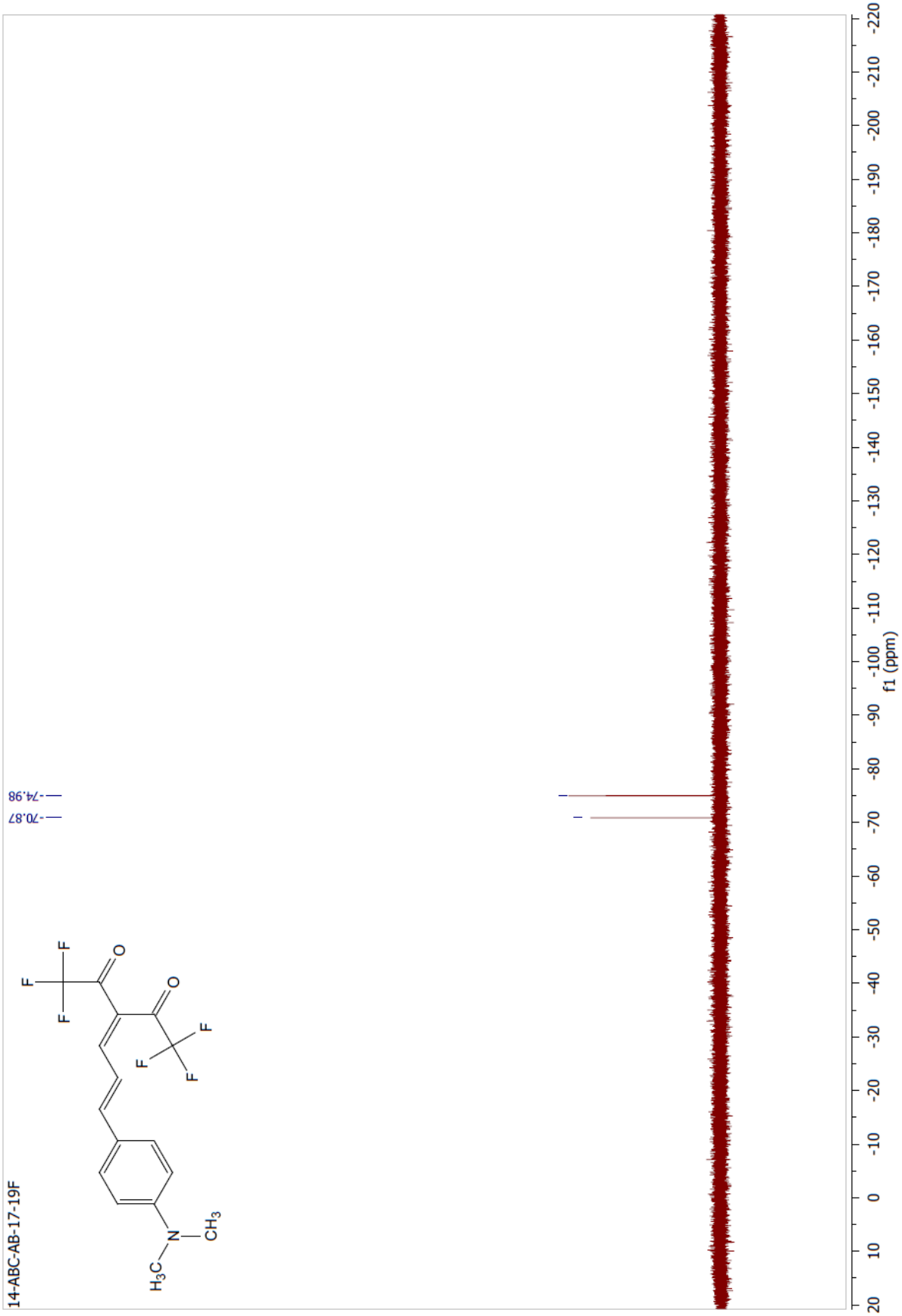

Figure S10: ^{19}F NMR spectrum of **A4** in $CDCl_3$.

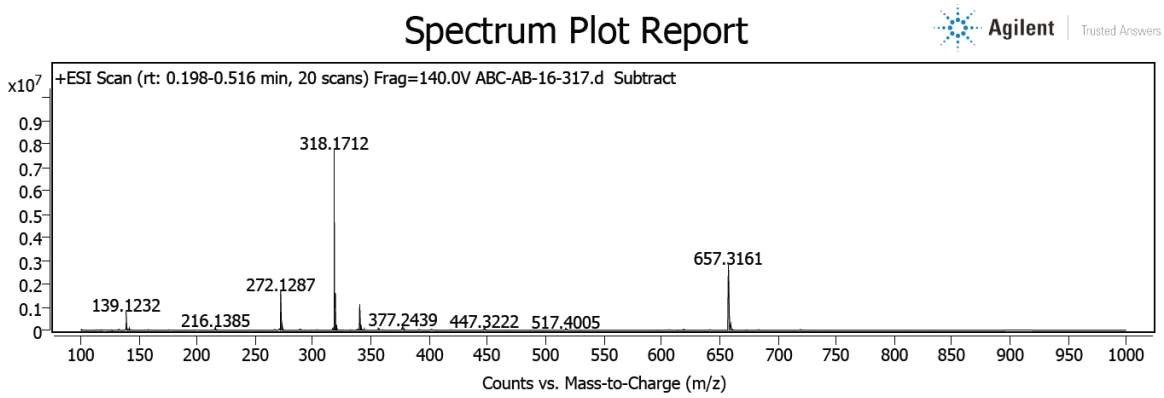

Figure S11: HRMS data of **A1** in MeOH.

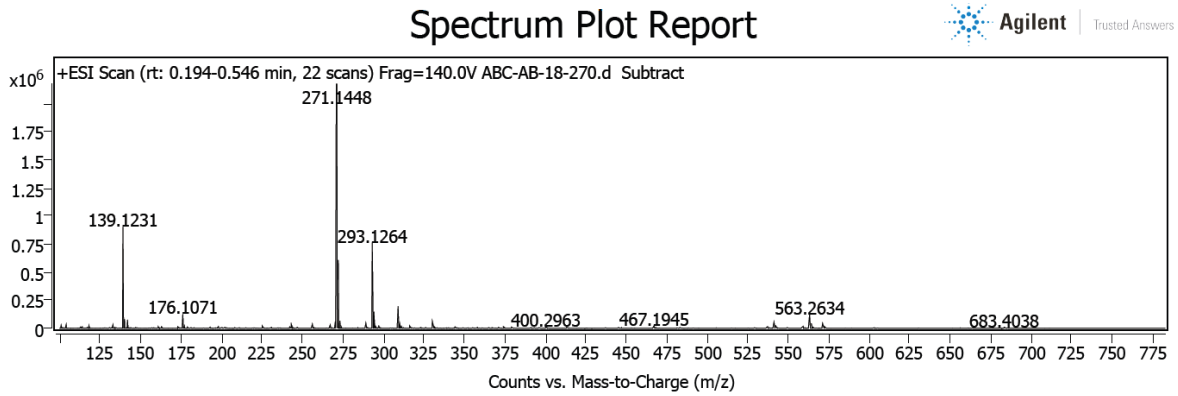

Figure S12: HRMS data of **A2** in MeOH.

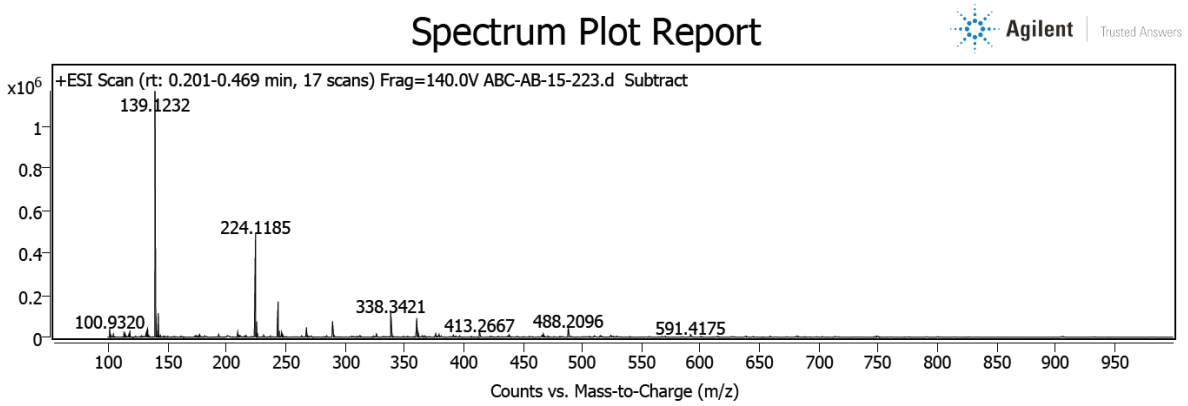

Figure S13: HRMS data of **A3** in MeOH.

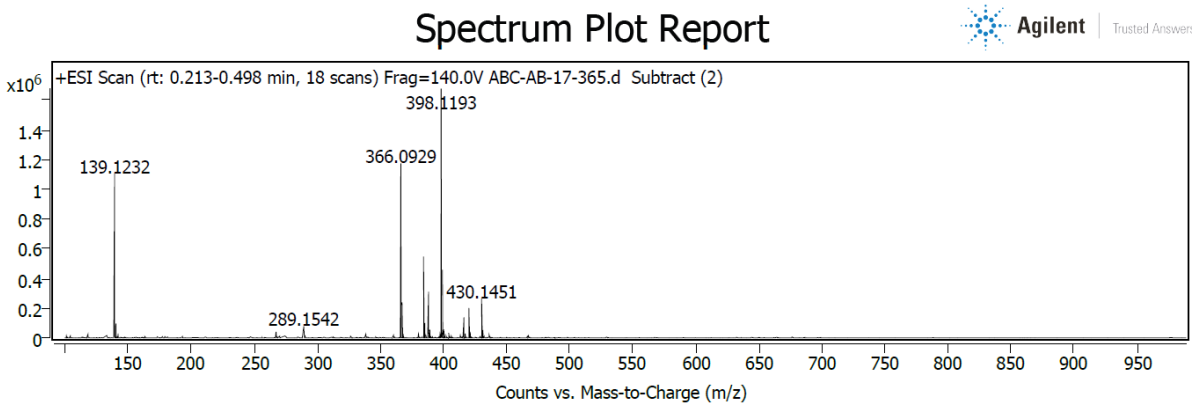

Figure S14: HRMS data of **A4** in MeOH.

Table S1: Comparison of the experimentally obtained absorption data with the theoretically obtained data using different functionals and using the basis set 6-31G+(d).[1-6]

Probe	Expt. (nm)	Theory (nm)							
		PBEPBE	B3LYP	CAM-B3LYP	M062X	BMK	ωB97XD	BHandHLYP	PBE1PBE
A4	522	529.81	496.46	468.4	474.03	471.14	465.08	449.22	485.33

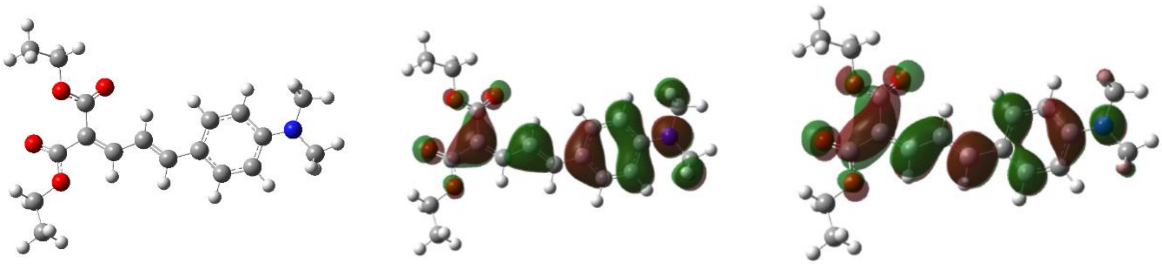

A1 **E_{HOMO}=-0.17725** **E_{LUMO}=-0.11259**

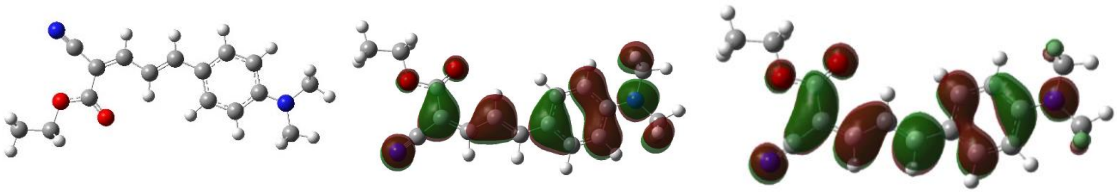

A2 **E_{HOMO}=-0.18204** **E_{LUMO}=-0.12025**

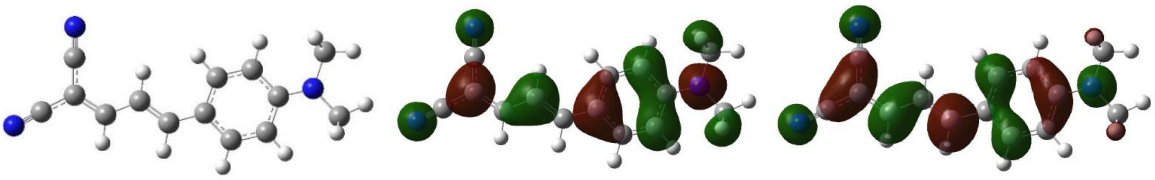

A3 **E_{HOMO}=-0.18501** **E_{LUMO}=-0.12425**

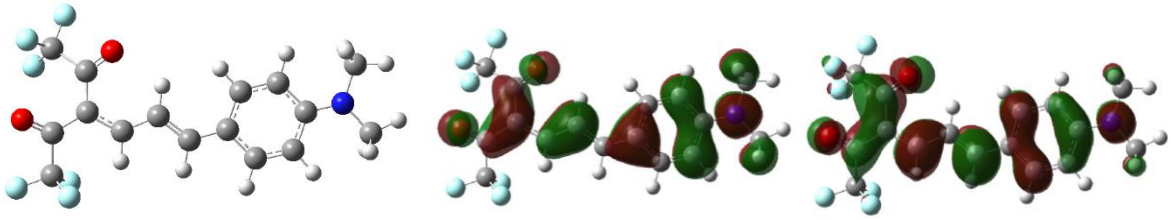

A4 **E_{HOMO}=-0.19358** **E_{LUMO}=-0.13692**

Figure S15: Energy optimized structures using PBEPBE Functional and 6-31+g (d) basis set and Frontier molecular orbital analysis of compounds **A1**, **A2**, **A3,** and **A4**.

Table S2: HOMO-LUMO energy gap as obtained from the frontier molecular orbital analysis of compounds **A1**, **A2**, **A3** and **A4**.

Probes	**ΔE**	
A1	**0.0646**	*** 27.2114 = 1.759eV**
A2	**0.0617**	*** 27.2114 = 1.681eV**
A3	**0.0607**	*** 27.2114 = 1.653eV**
A4	**0.0566**	*** 27.2114 = 1.5417eV**

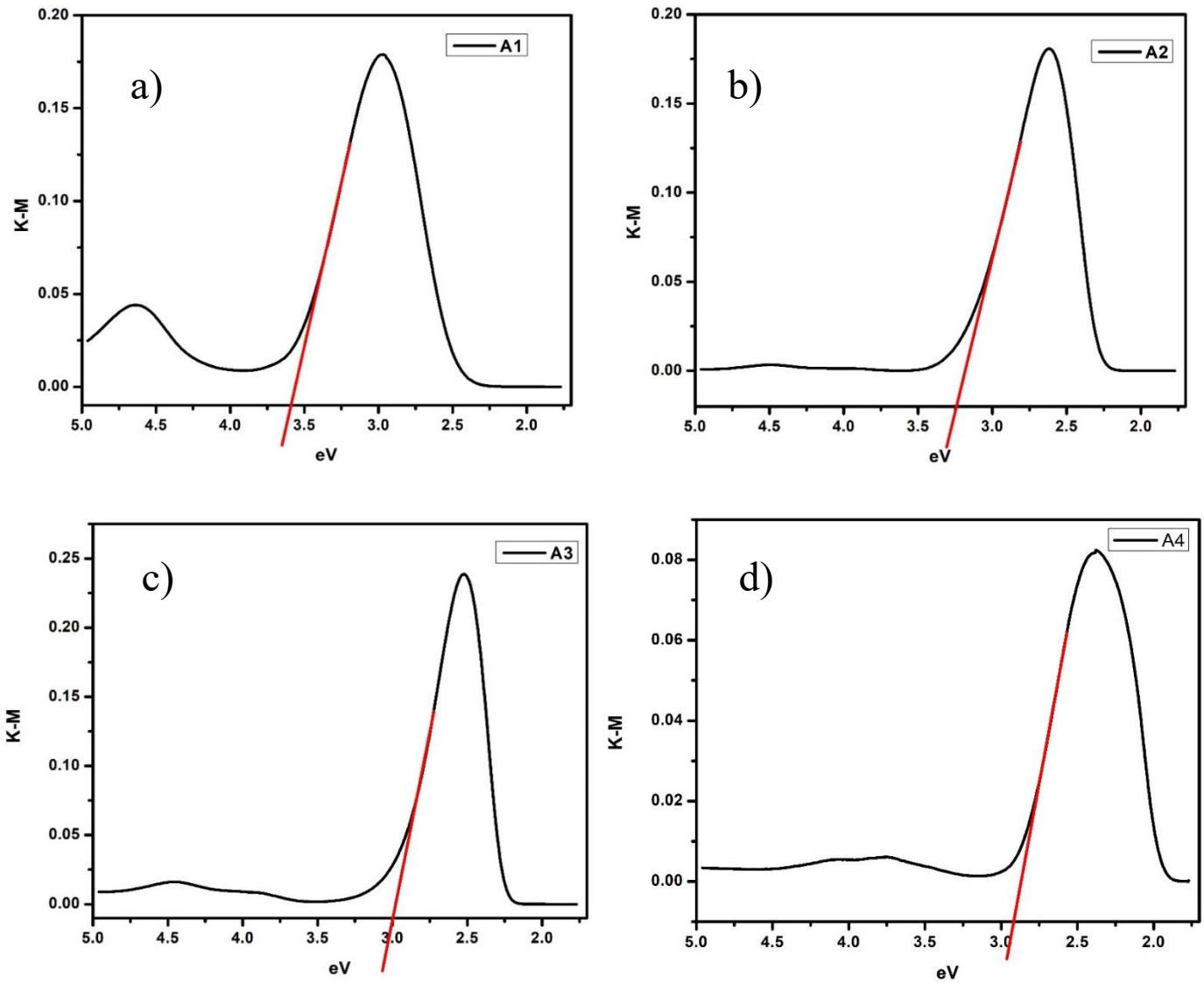

Figure S16: Experimentally obtained band gap for the probes A1, A2, A3 and A4 using the Tauc plot. The band gap energies being **A1:** 3.59eV**, A2:** 3.24eV**, A3:** 3 eV and **A4:** 2.91eV.[7-9]

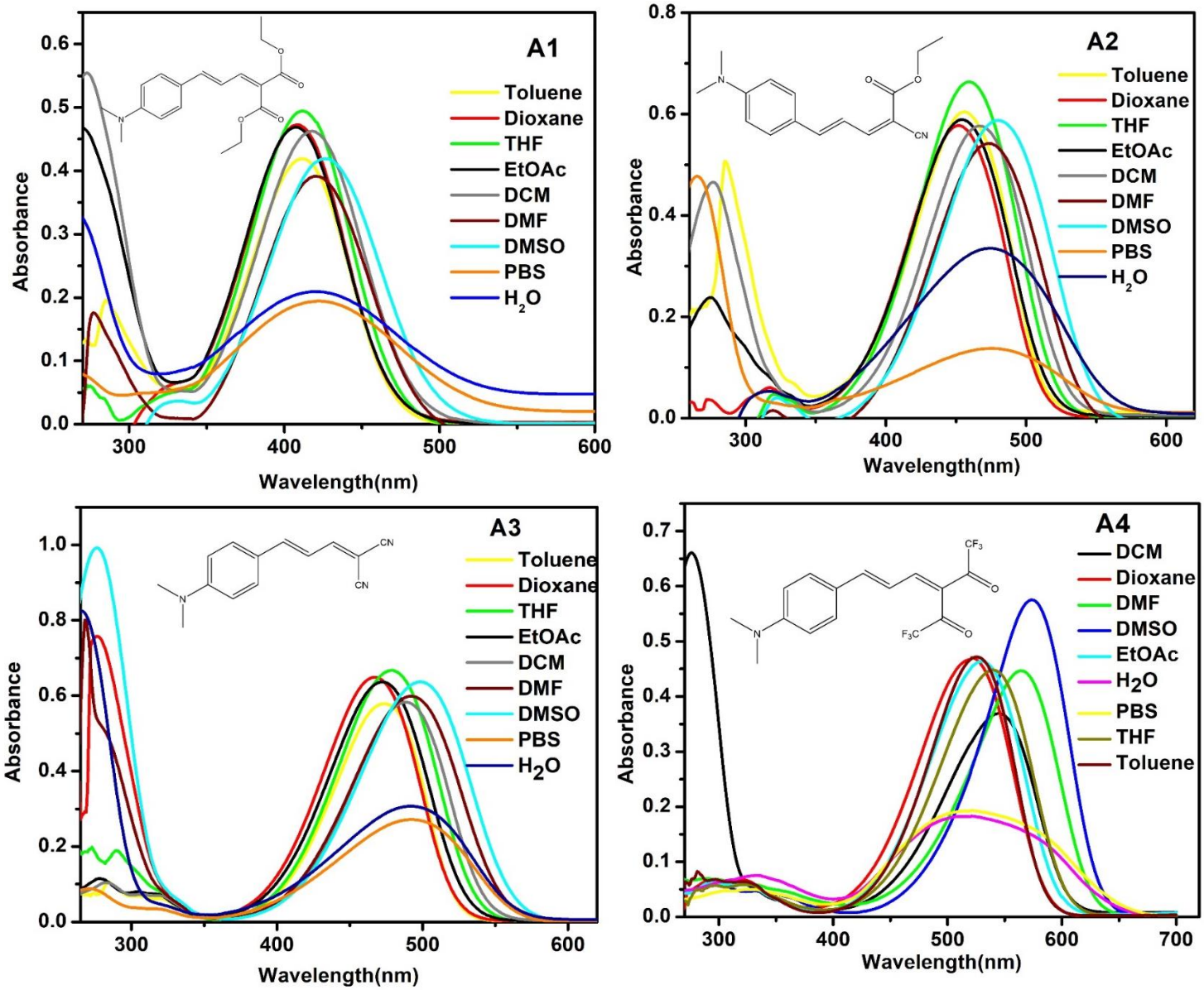

Figure S17: The Absorption spectra of **A1**, **A2**, **A3**, and **A4** in solvents of different polarities.

Table S3: Experimental spectral absorption and emission maxima Stokes shifts and molar extinction coefficient values of **A1** in different solvents.

Solvent	***Dielectric constant***	***λ_{nm} (absorbance) for A1***	***ε (M^{-1} cm^{-1})***	***λ_{nm} (emission) for A1***	***Stokes shift (nm)***
Toluene	2.38	411	41840	516	105
Dioxane	2.25	409	47150	525	116
THF	7.58	411	49460	538	127

EtOAc	6.02	407	46810	534	127
DCM	8.93	417	46350	545	128
DMF	36.7	420	39340	564	144
DMSO	46.7	426	42130	574	148
Water	80.1	420	21270	590	170

Table S4: Experimental spectral absorption and emission maxima Stokes shifts and molar extinction coefficient values of **A2** in different solvents.

Solvent	***Dielectric constant***	$\lambda_{nm\ (absorbance)\ for}$ ***A2***	ε ***(M^{-1} cm^{-1})***	$\lambda_{nm\ (emission)\ for}$ ***A2***	***Stokes shift (nm)***
Toluene	2.38	456	60070	532	76
Dioxane	2.25	451	57660	540	89
THF	7.58	459	66230	553	94
EtOAc	6.02	454	58860	550	96
DCM	8.93	467	58016	557	90
DMF	36.7	473	54236	580	107
DMSO	46.7	480	58803	587	107
Water	80.1	476	33367	592	116

Table S5: Experimental spectral absorption and emission maxima Stokes shifts and molar extinction coefficient values of **A3** in different solvents.

Solvent	***Dielectric constant***	$\lambda_{nm\ (absorbance)\ for}$ ***A3***	ε ***(M^{-1} cm^{-1})***	$\lambda_{nm\ (emission)\ for}$ ***A3***	***Stokes shift (nm)***
Toluene	2.38	473	57869	535	62
Dioxane	2.25	467	65020	546	79
THF	7.58	478	66823	562	84
EtOAc	6.02	472	63758	554	82

DCM	8.93	489	58109	565	76
DMF	36.7	492	60062	586	94
DMSO	46.7	499	63758	590	91
Water	80.1	492	30977	587	95

Table S6: Quantum Yield of A4 in solvents of varying polarities and in the presence of HSA.

The quantum yield of A4	**Solvent/ Medium**
0.00041	PBS Buffer
0.02051	Toluene
0.0719	HSA(10μM) in PBS

Table S7: A comparison of the results obtained for the TD-DFT calculations performed using linear response and state-specific approaches with the experimental data.

Probe A4	**Absorption**	**Emission**
Theoretically obtained using Linear response approach	529.8nm	608.94nm
Theoretically obtained using a State-specific approach	501.55nm	646.88nm
Experimentally obtained	522nm	623nm

Table S8: The optimized molecular structure of **A4** was determined using DFT (density functional theory) and TD (time-dependent)-DFT studies using PBEPBE Functional and 6-31+g (d) basis set. The theoretically obtained results closely match the experimentally obtained results.

Probe A4	**Absorption**	**Emission**
Theoretically obtained	529.8nm *f* = 1.0475	608.94nm *f* = 1.3703
Experimentally obtained	522nm	623nm

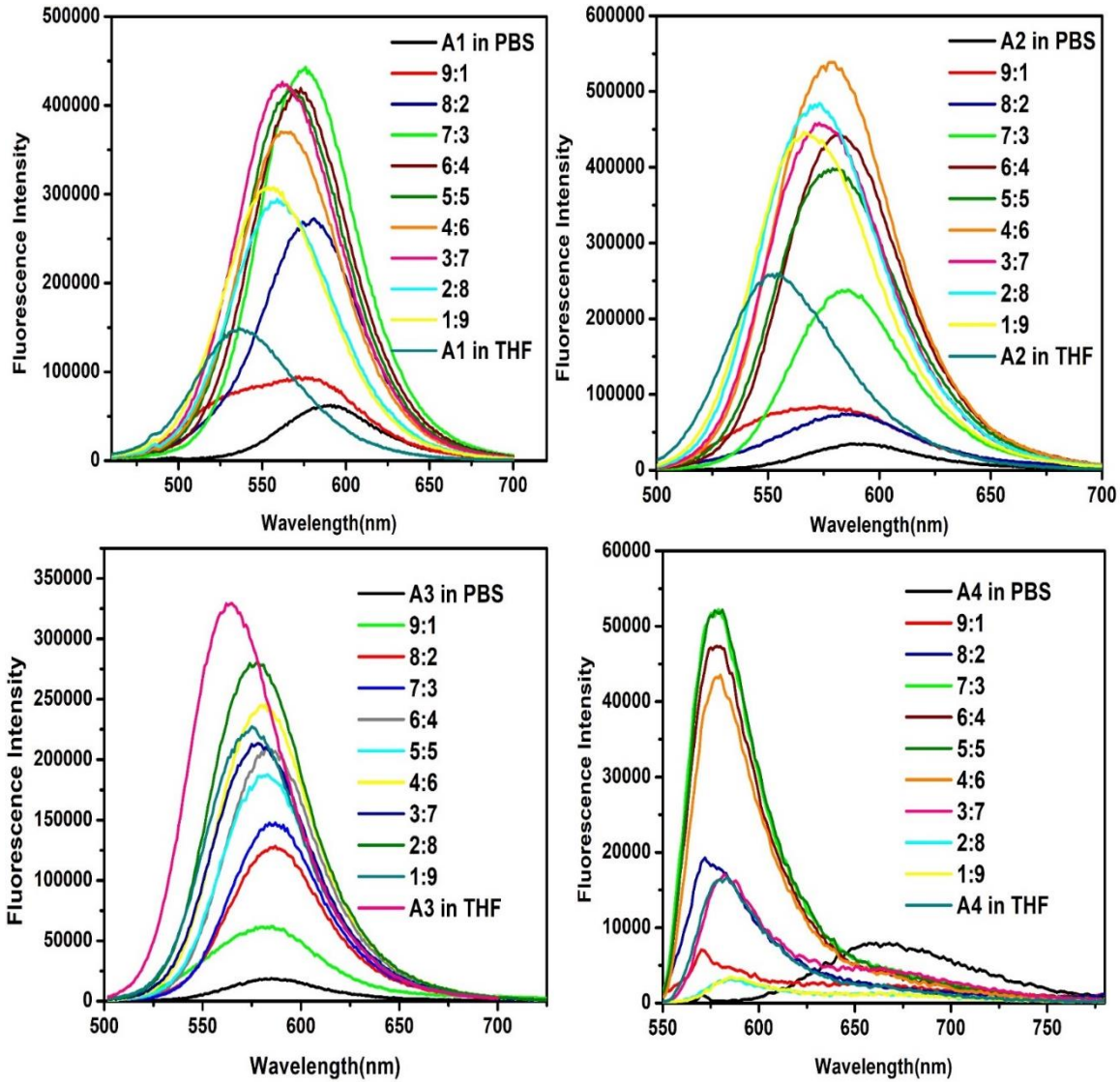

Figure S18: Fluorescence spectra of **A1**, **A2**, **A3**, and **A4** (10μM) in different ratios of THF/PBS mixture.

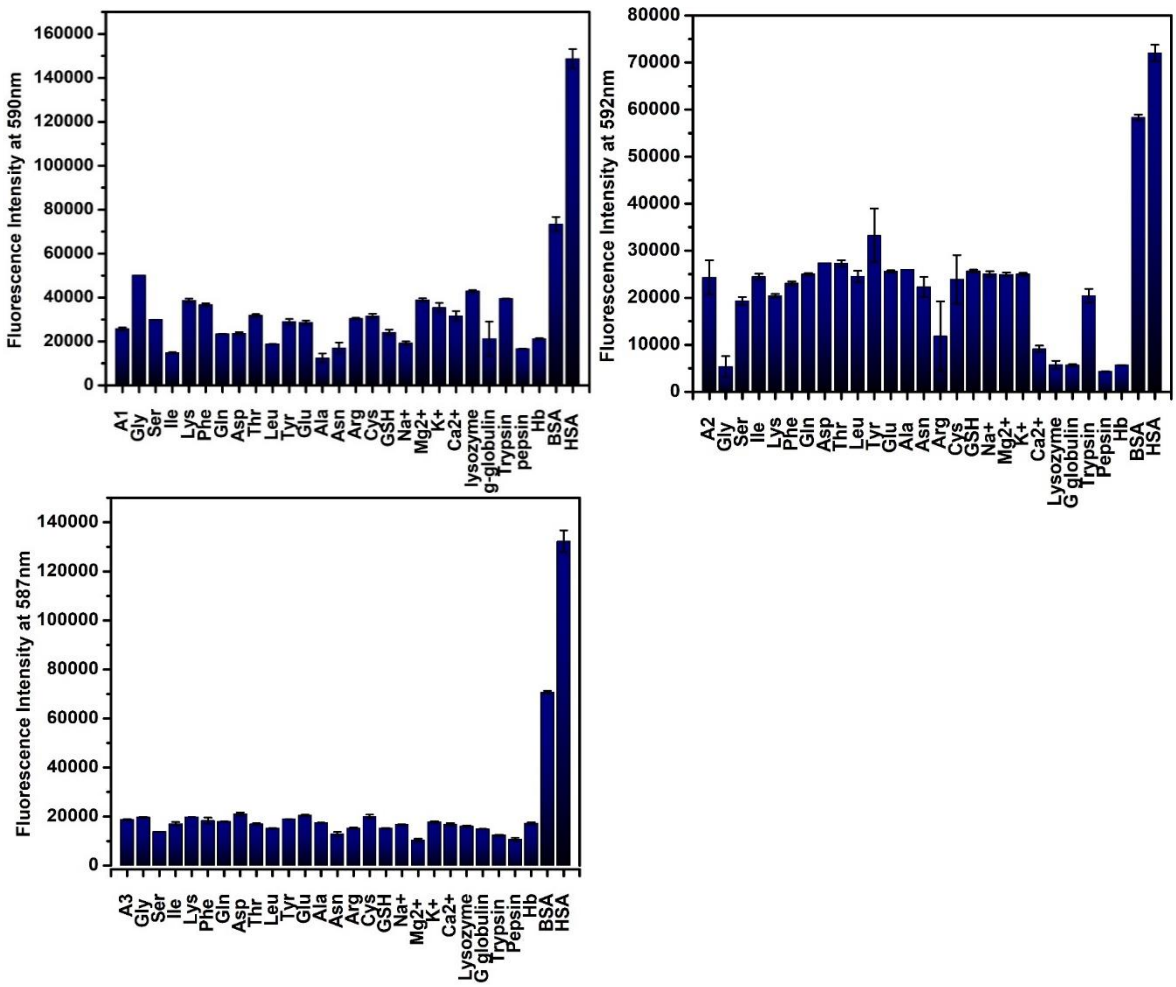

Figure S19: Bar plot showing the results of selectivity experiments of A1, A2, and A3 (5μM) against 100μM of amino acids and cations, and 10μM of proteins.

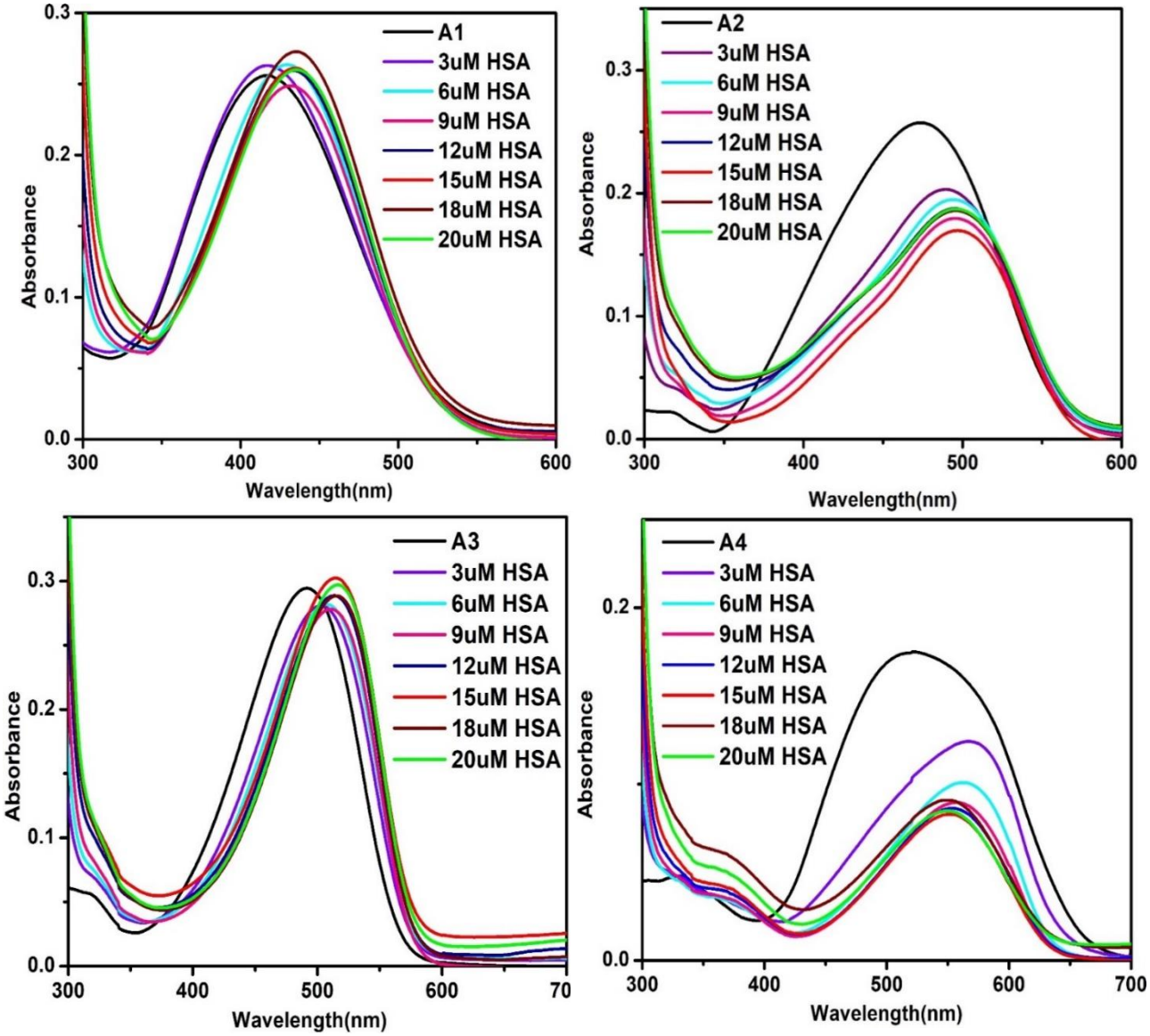

Figure S20: Absorption spectra showing interaction of probes **A1**, **A2**, **A3,** and **A4** with increasing concentrations of HSA.

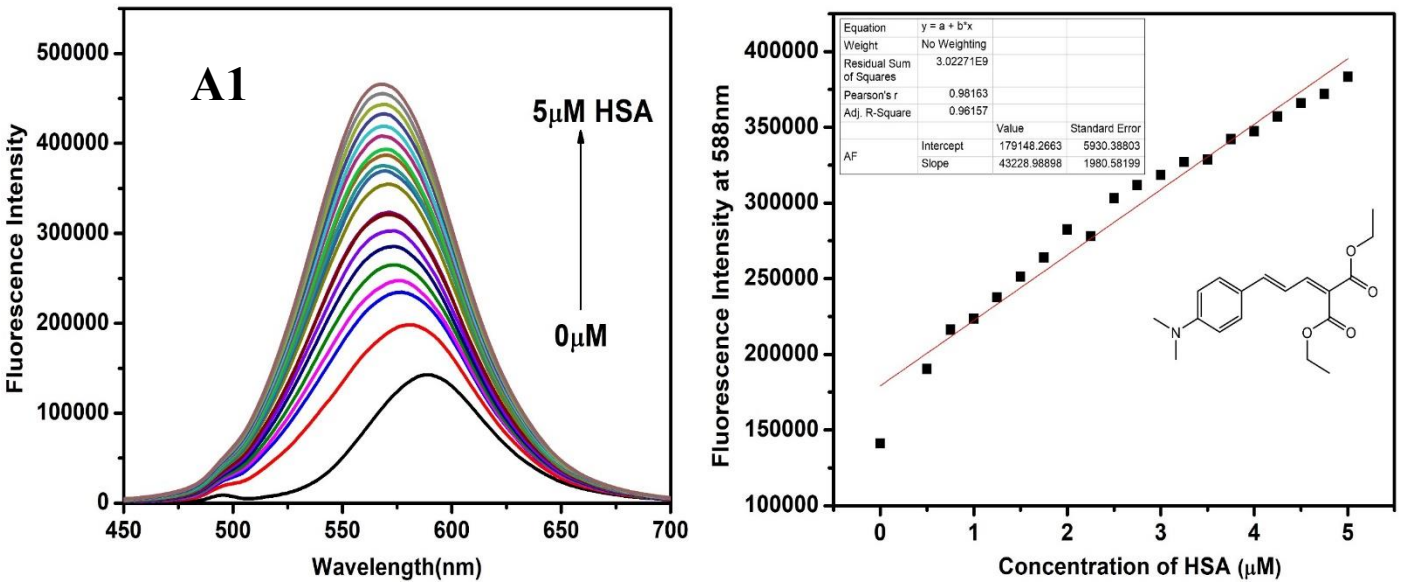

Figure S21: Fluorescence titration experiment showing the interaction of probe **A1** (5μM) in the presence of HSA (0 to 5μM) in PBS buffer (pH=7.4). Calibration curve at λem=588 nm for calculating the detection limit of HSA using **A1**.

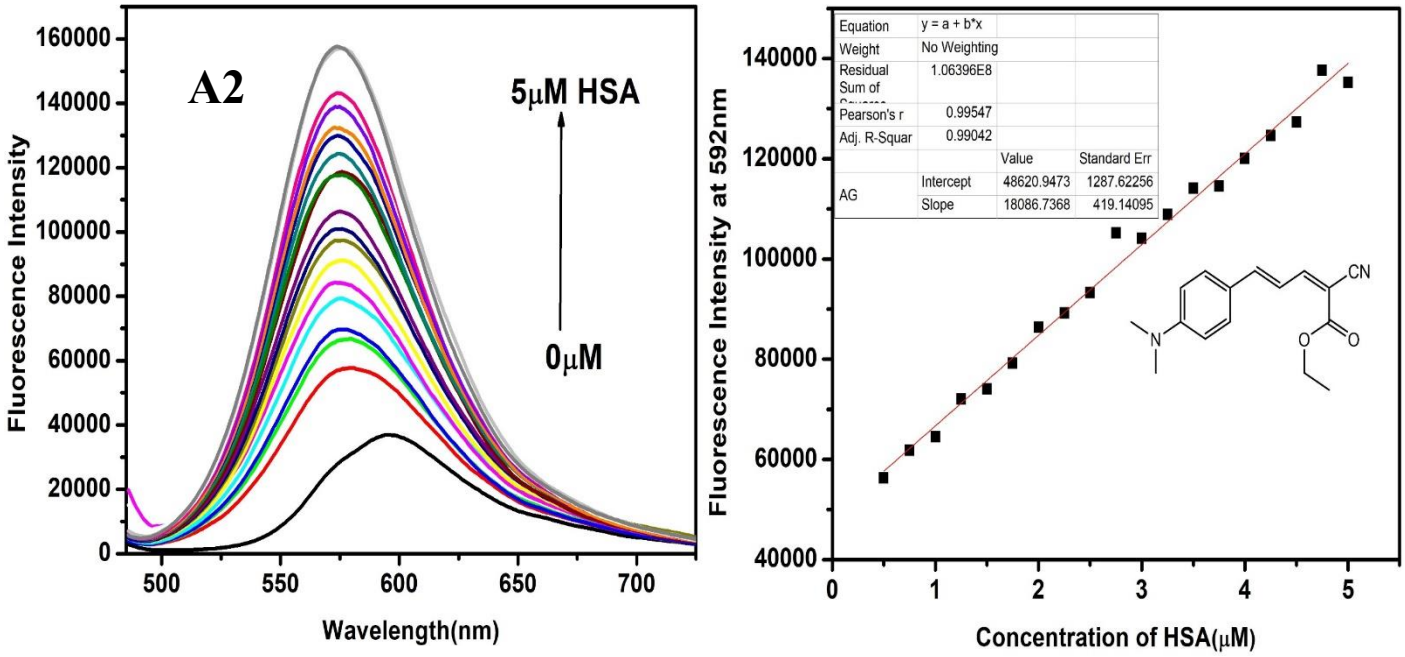

Figure S22: Fluorescence titration experiment showing the interaction of probe **A2** (5μM) in the presence of HSA (0 to 5μM) in PBS buffer (pH=7.4). Calibration curve at λem=592 nm for calculating the detection limit of HSA using **A2**.

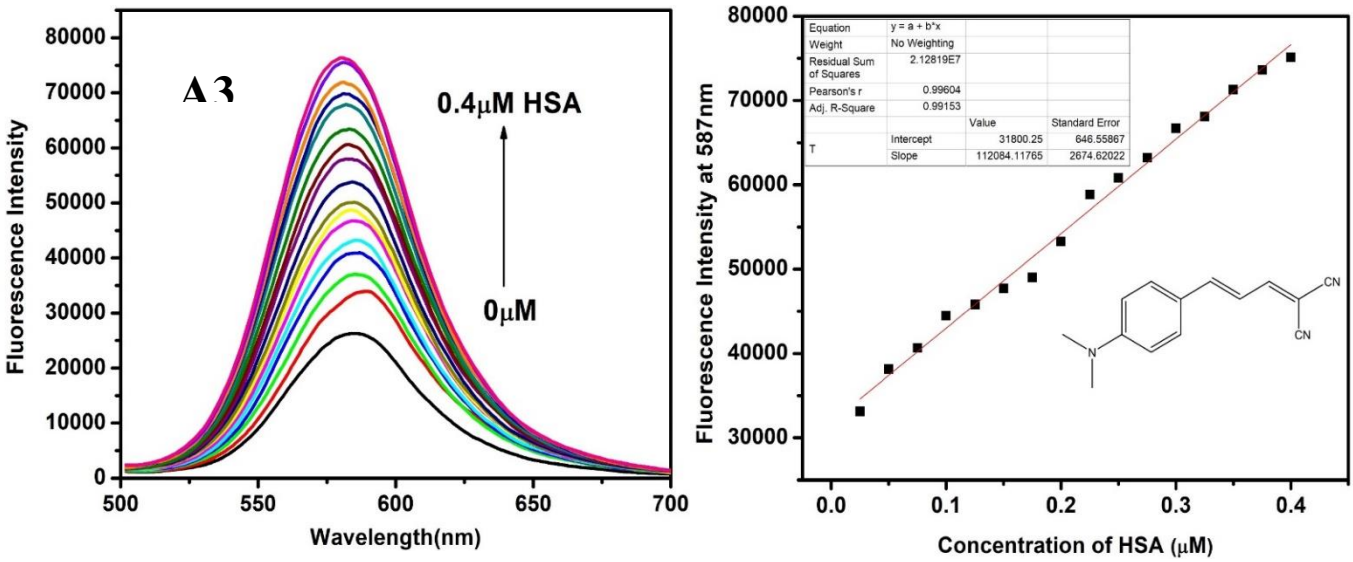

Figure S23: Fluorescence titration experiment showing the interaction of probe **A3** (5μM) in the presence of HSA (0 to 0.4μM) in PBS buffer (pH=7.4). Calibration curve at λem=587 nm for calculating the detection limit of HSA using **A3**.

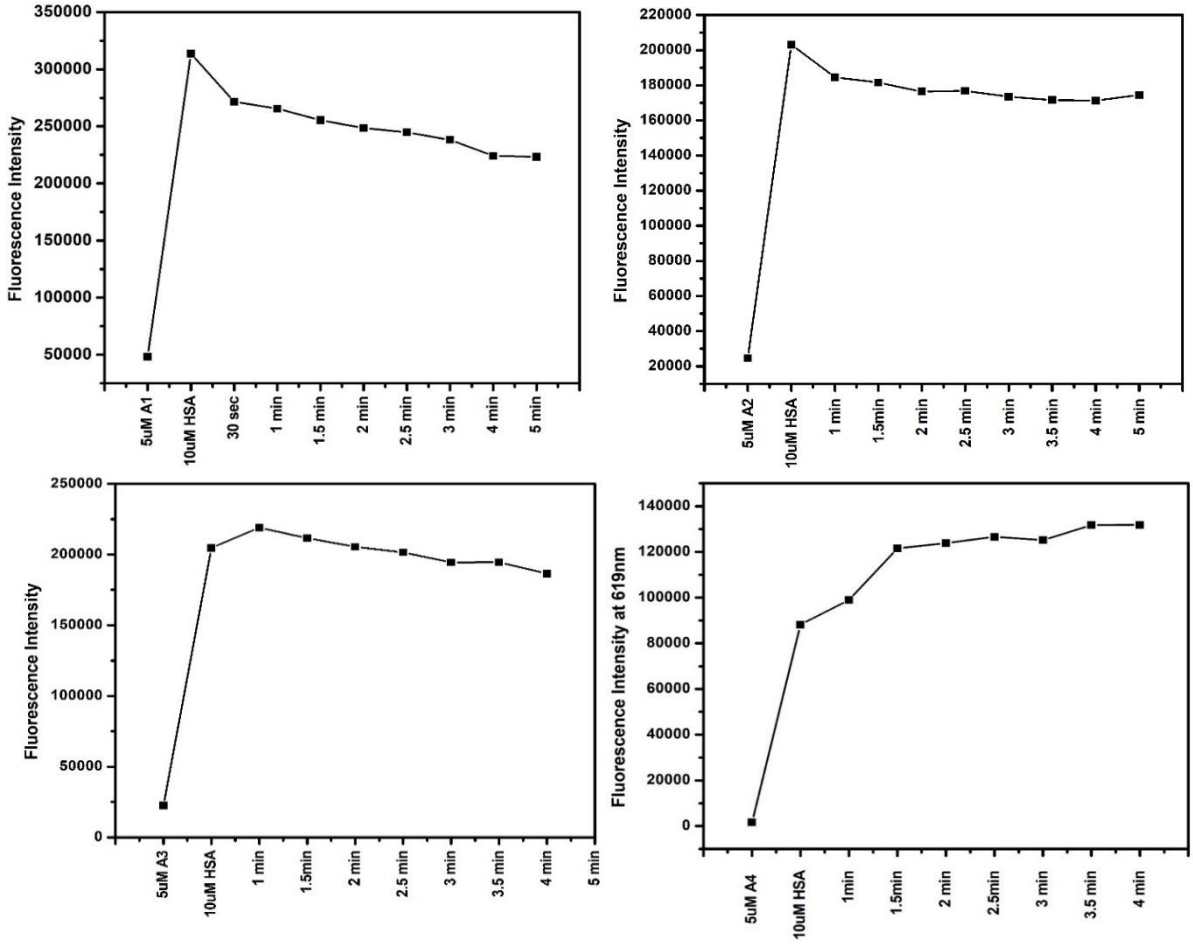

Figure S24: Signal saturation experiments monitoring the fluorescence enhancement of PROBE-HSA conjugate evolve over time.

Table S9: A comparison of the probes for HSA reported in recent times with this work.

PROBE	DETECTION LIMIT	DETECTION TIME
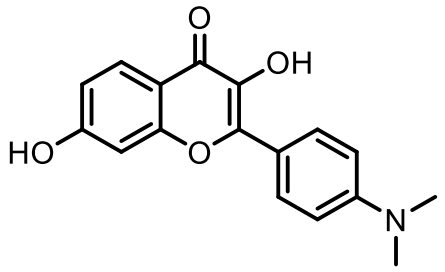 Ref: 10	21nM	30 Sec
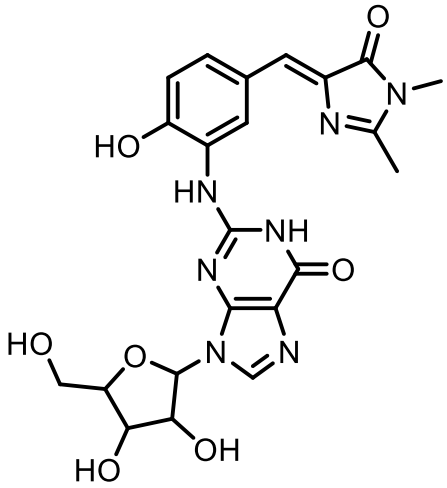 Ref: 11	22.72 pM	< 1min
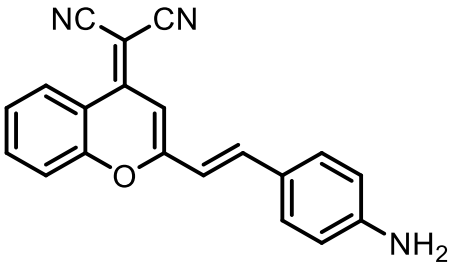 Ref: 12	28.6 nM	30 sec
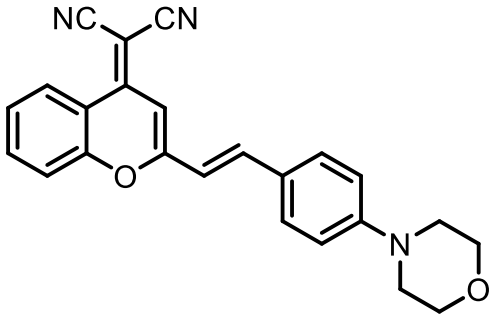 Ref: 13	3.78 nM	15min
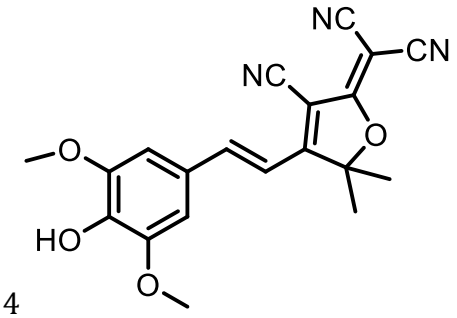 Ref: 14	15.15 nM	1 min

Ref:15 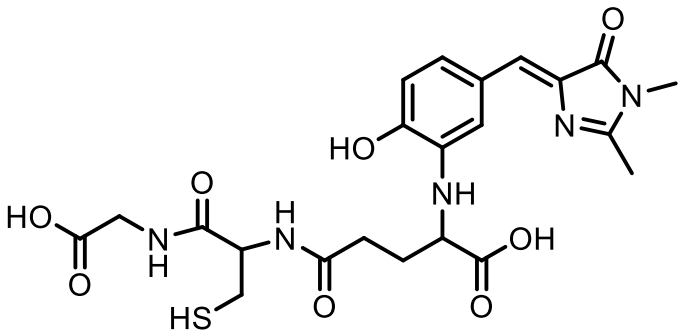	3 pM	-
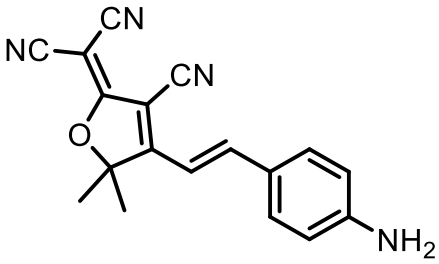 Ref:16	37.87 nM	3 sec
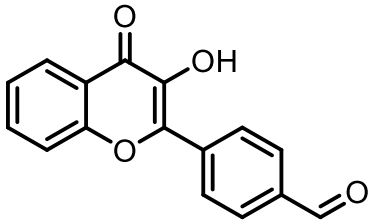 Ref:17	20.7 nM	1 min
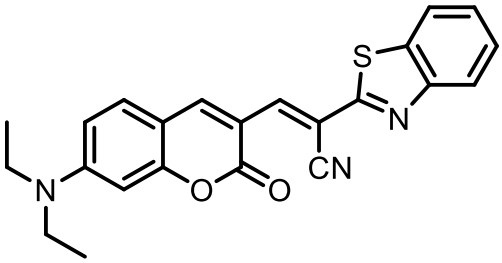 Ref:18	287.87 pM	3 min
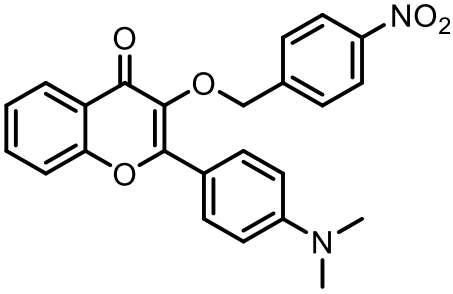 Ref:19	32 nM	10 sec
This work	1.36nM	90 sec

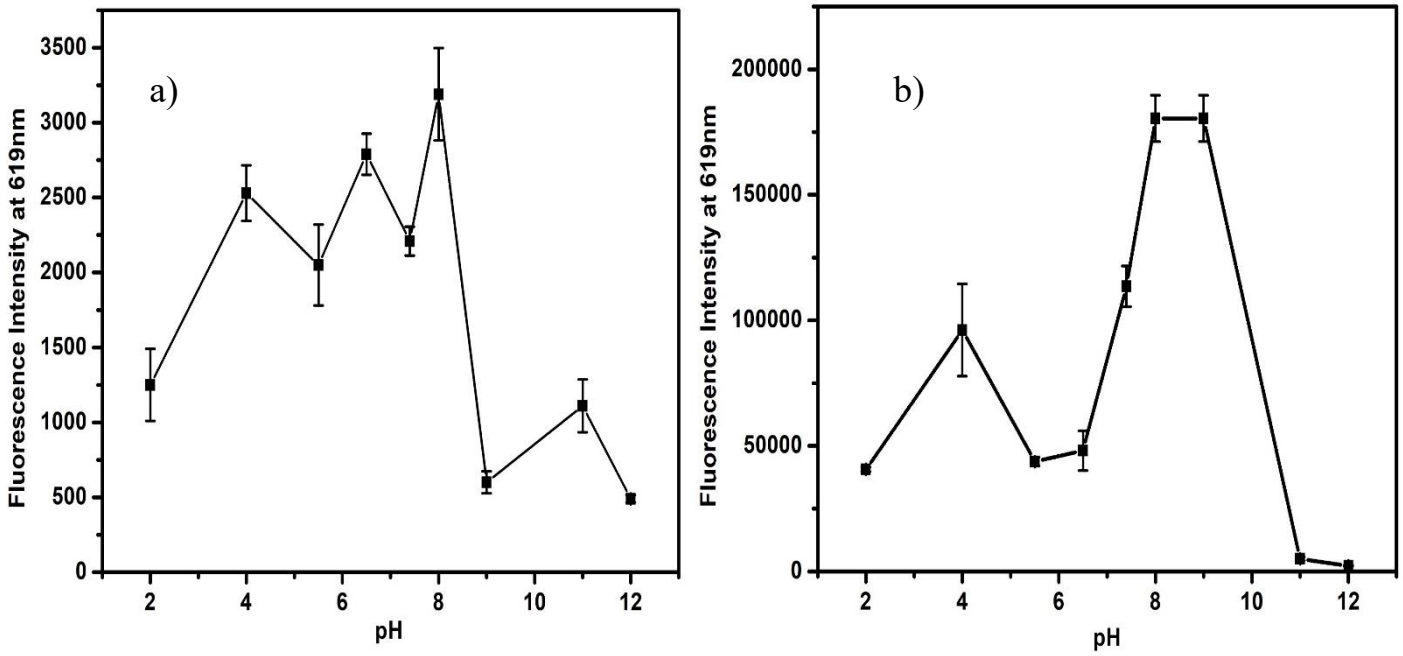

Figure S25: Effect of pH on the a) fluorescence emission of A4 b) fluorescence emission of A4-HSA ensemble.

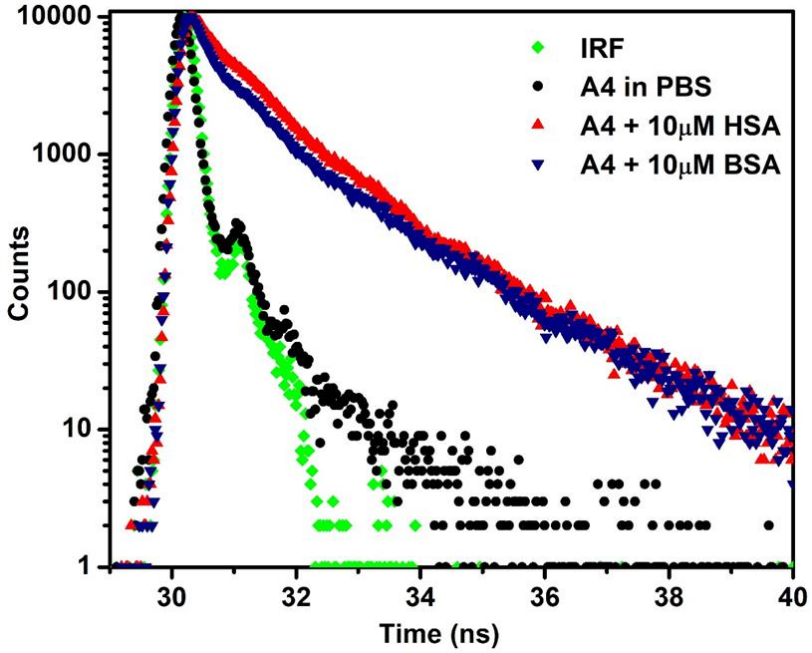

Figure S26: Time-resolved fluorescence decays of A4 in the absence and presence of HSA and BSA. The green-colored profile is the instrumental response function. λ_{ex}= 510 nm.

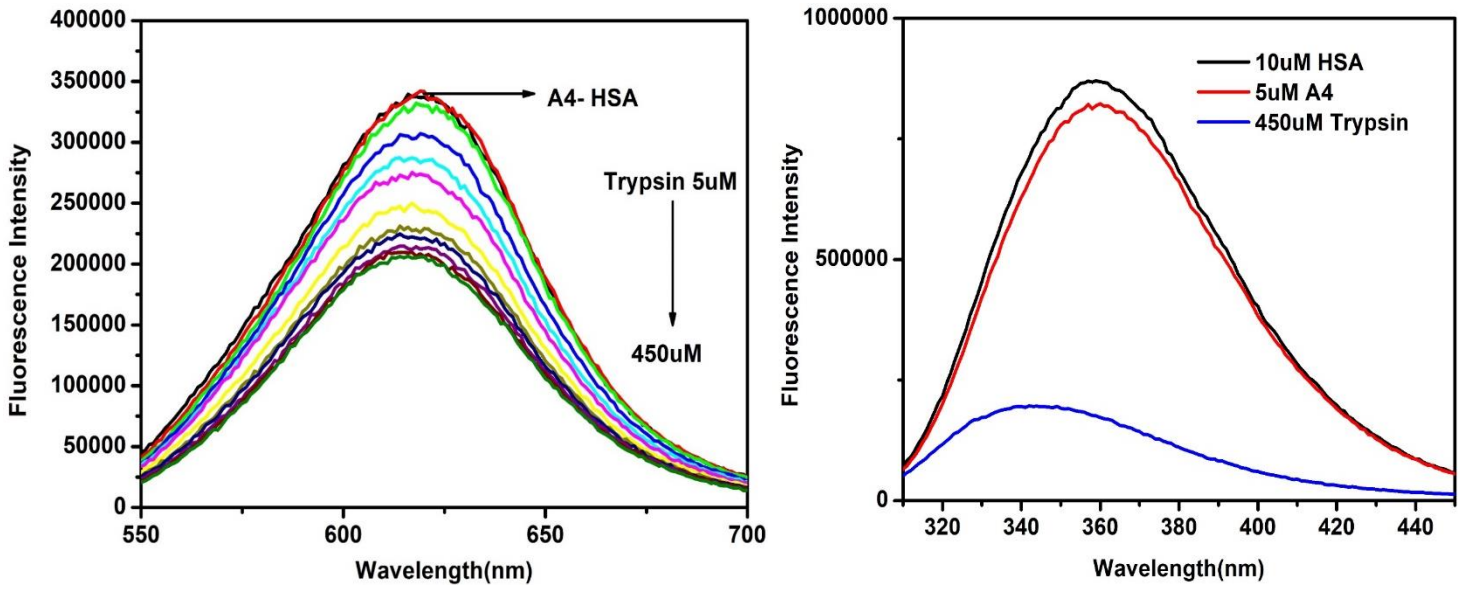

Figure S27: Fluorescence spectra of A4- HSA ensemble in the presence of increasing concentrations of trypsin. **a)** Effect of trypsin on the protein's fluorescence intensity **b)** Effect of trypsin on the probe A4's fluorescence intensity.

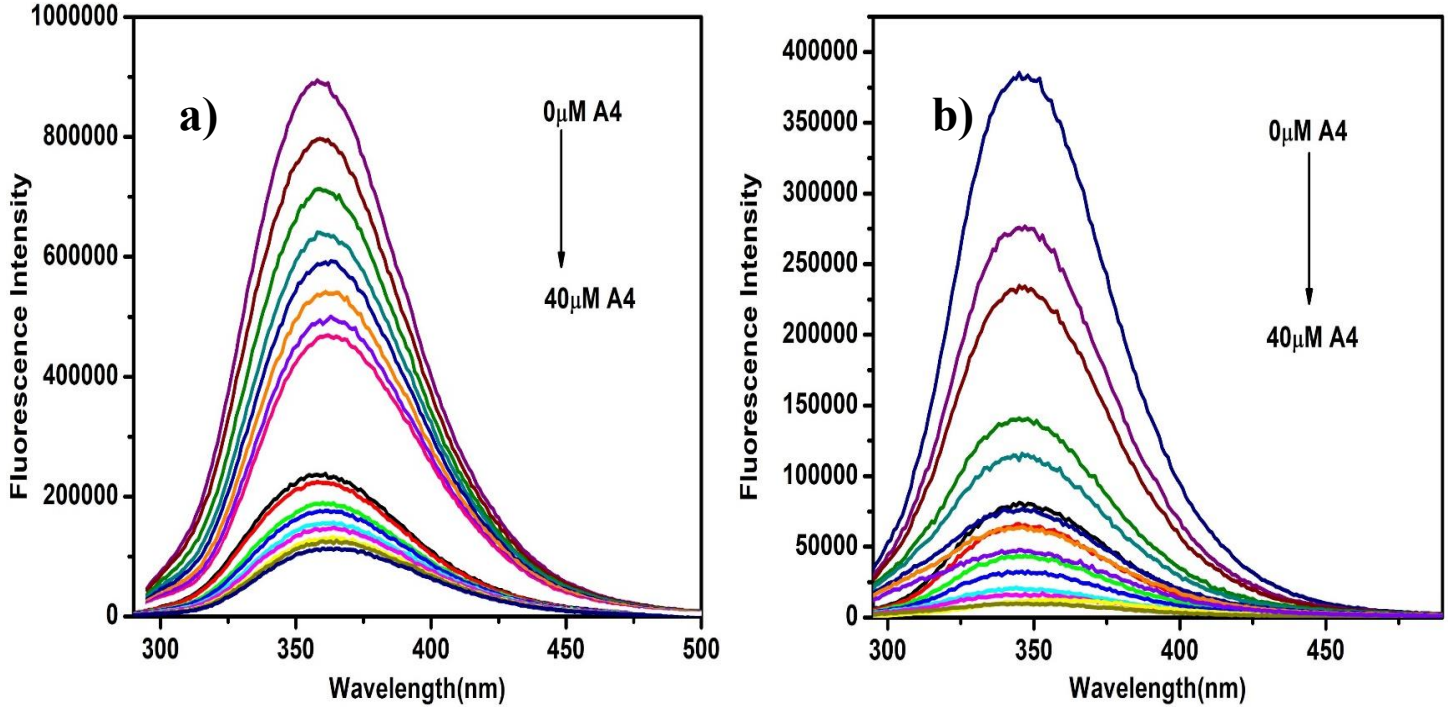

Figure S28: a) HSA Fluorescence quenching by the addition of increasing concentrations of A4. Tyrosine and tryptophan fluorescence monitored. **b) BSA** Fluorescence quenching by the addition of increasing concentrations of A4.

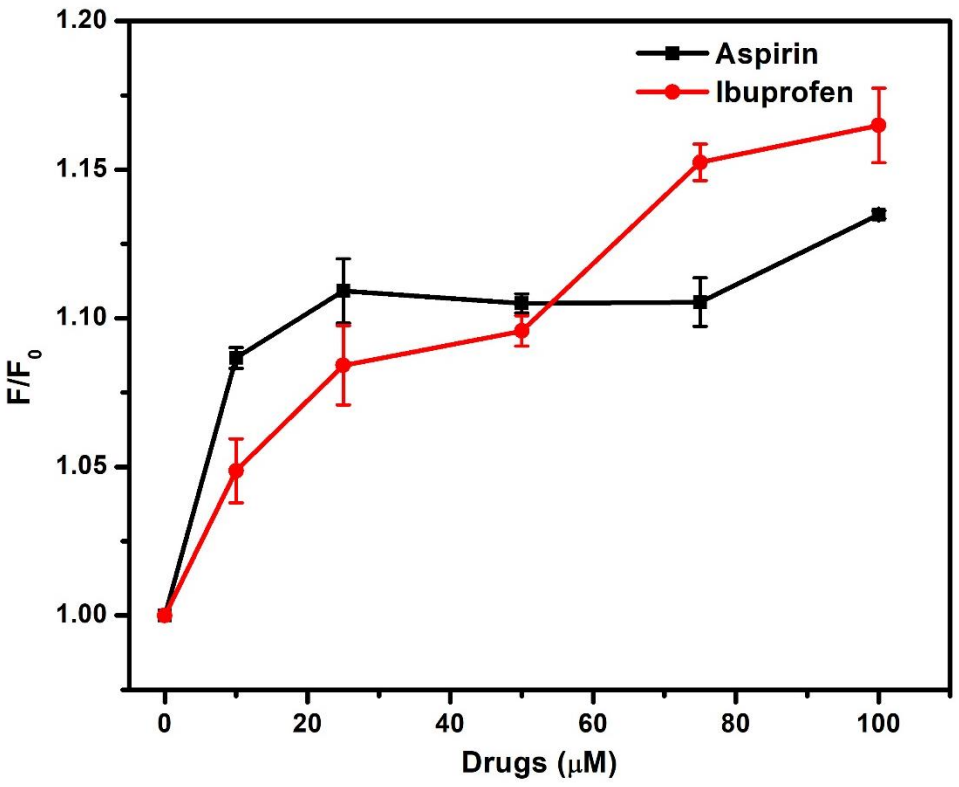

Figure S29: Displacement assay of A4 where site-specific drugs were tested against the complex of HSA-A4. The expanded version of aspirin and ibuprofen.

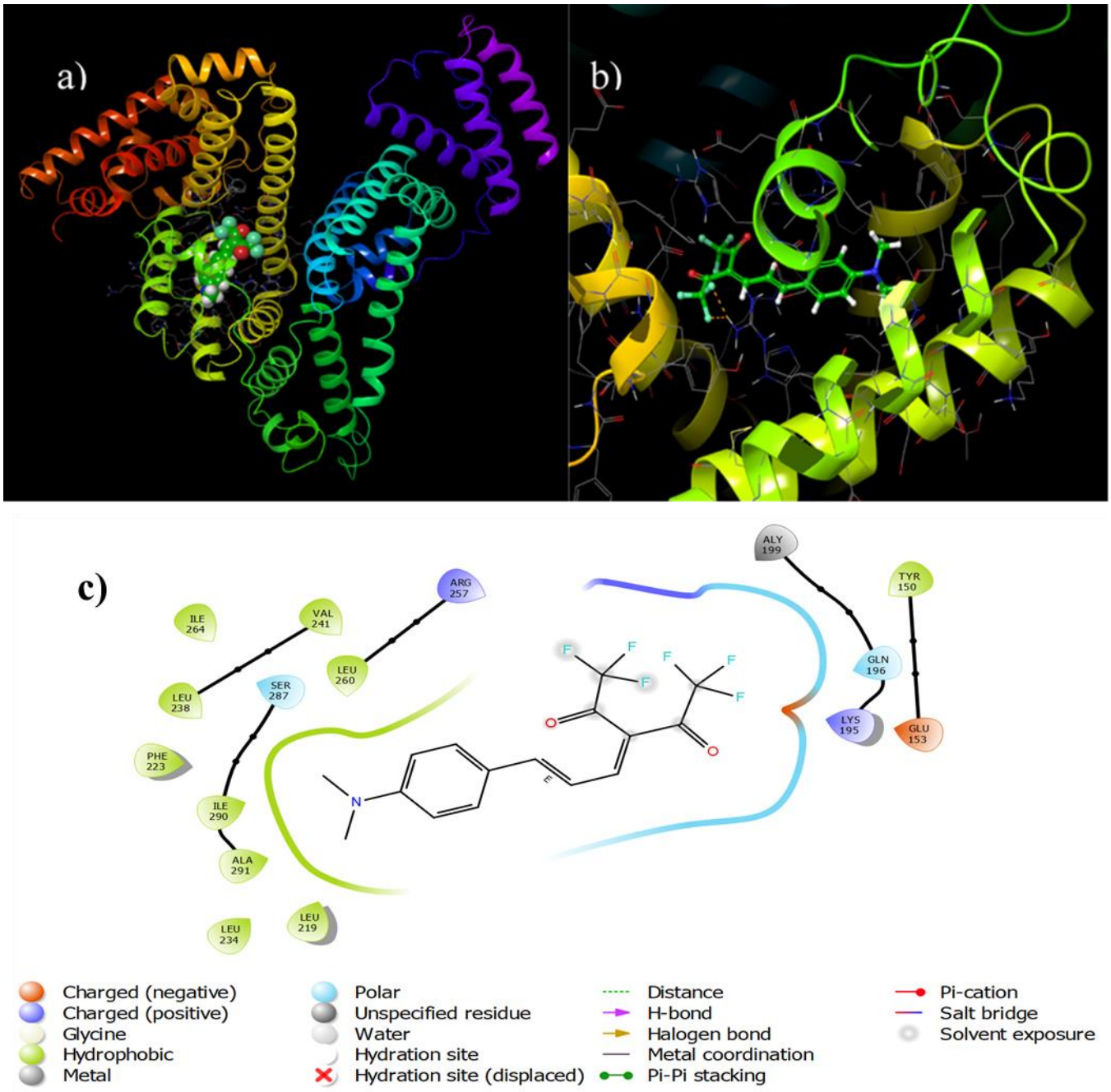

Figure S30: Binding interaction between A4 and the site B of 2I2Z. **a)** Shows the location of A4 in the protein. **b)** It shows the zoomed-in view of the A4 interaction with **HSA**. **c)** Lig-plot corresponding to the interaction between A4 and amino acids of the site B of 2I2Z.

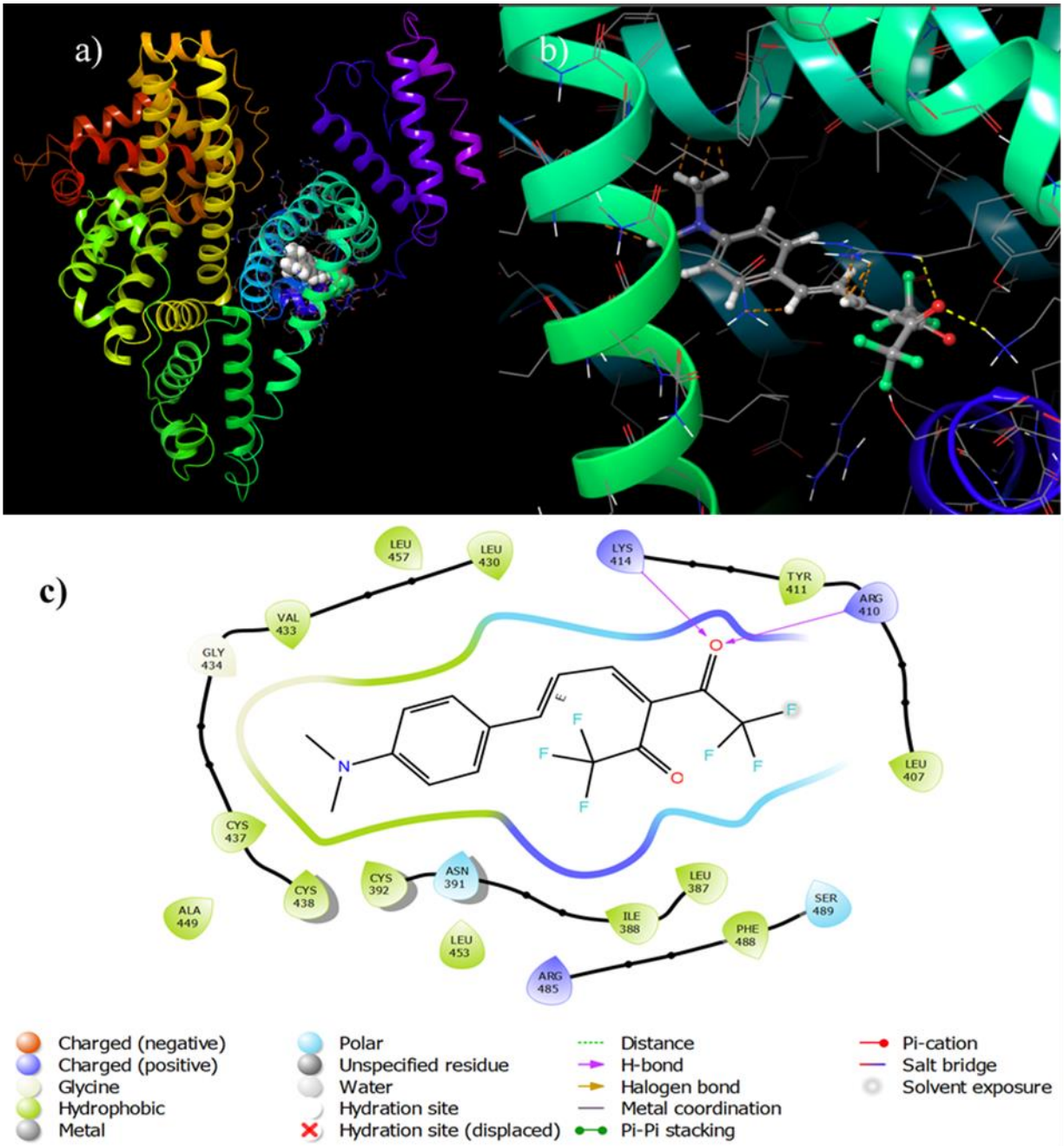

Figure S31: Binding interaction between A4 and the site C of 2BXG. **a)** Shows the location of A4 in the protein. **b)** It shows the zoomed-in view of the A4 interaction with **HSA**. **c)** Lig-plot corresponding to the interaction between A4 and amino acids of the site C of 2BXG.

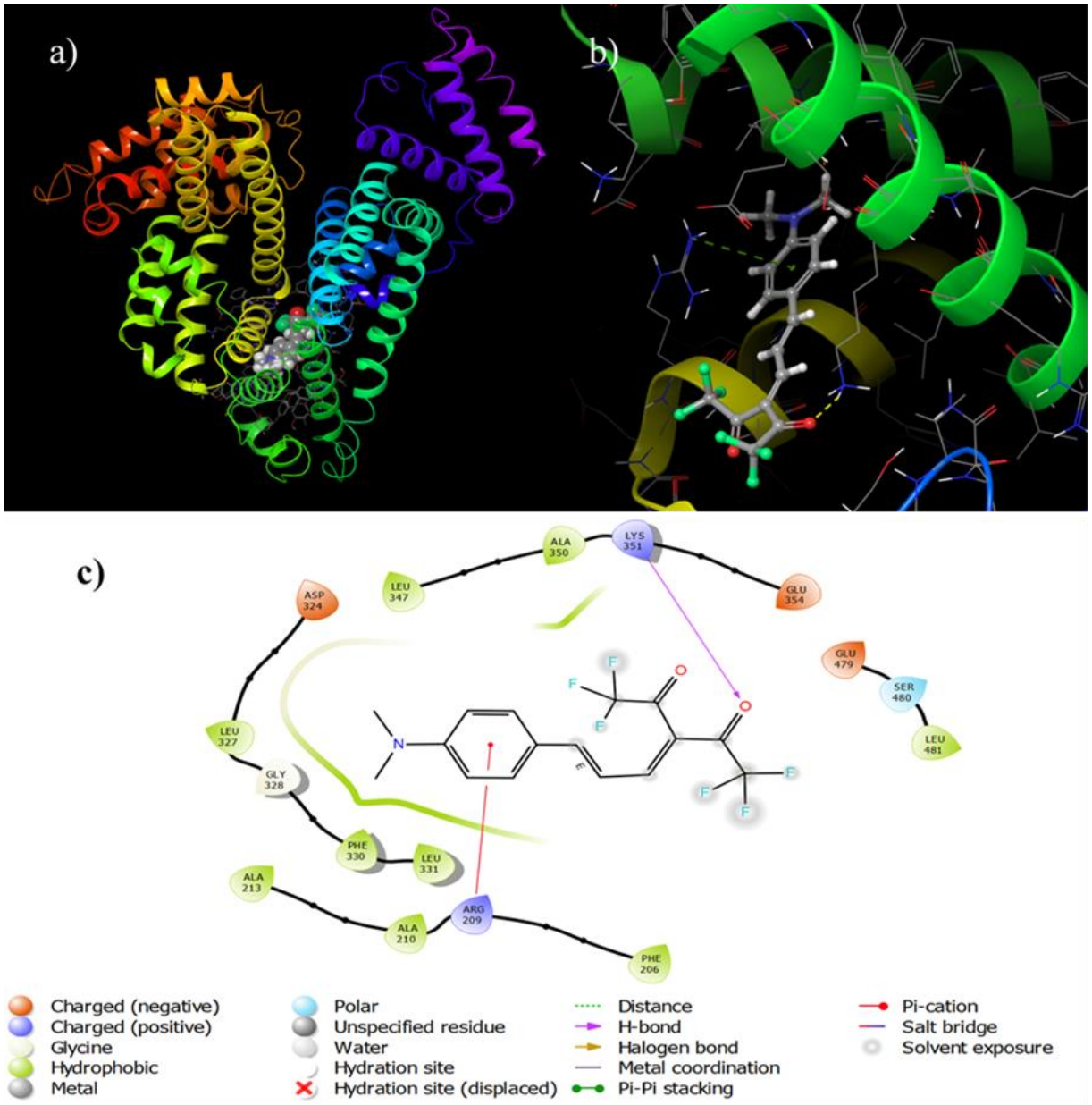

Figure S32: Binding interaction between A4 and the site D of 2BXG. **a)** Shows the location of A4 in the protein. **b)** It shows the zoomed-in view of the A4 interaction with **HSA**. **c)** Lig-plot corresponding to the interaction between A4 and amino acids of the site D of 2BXG.

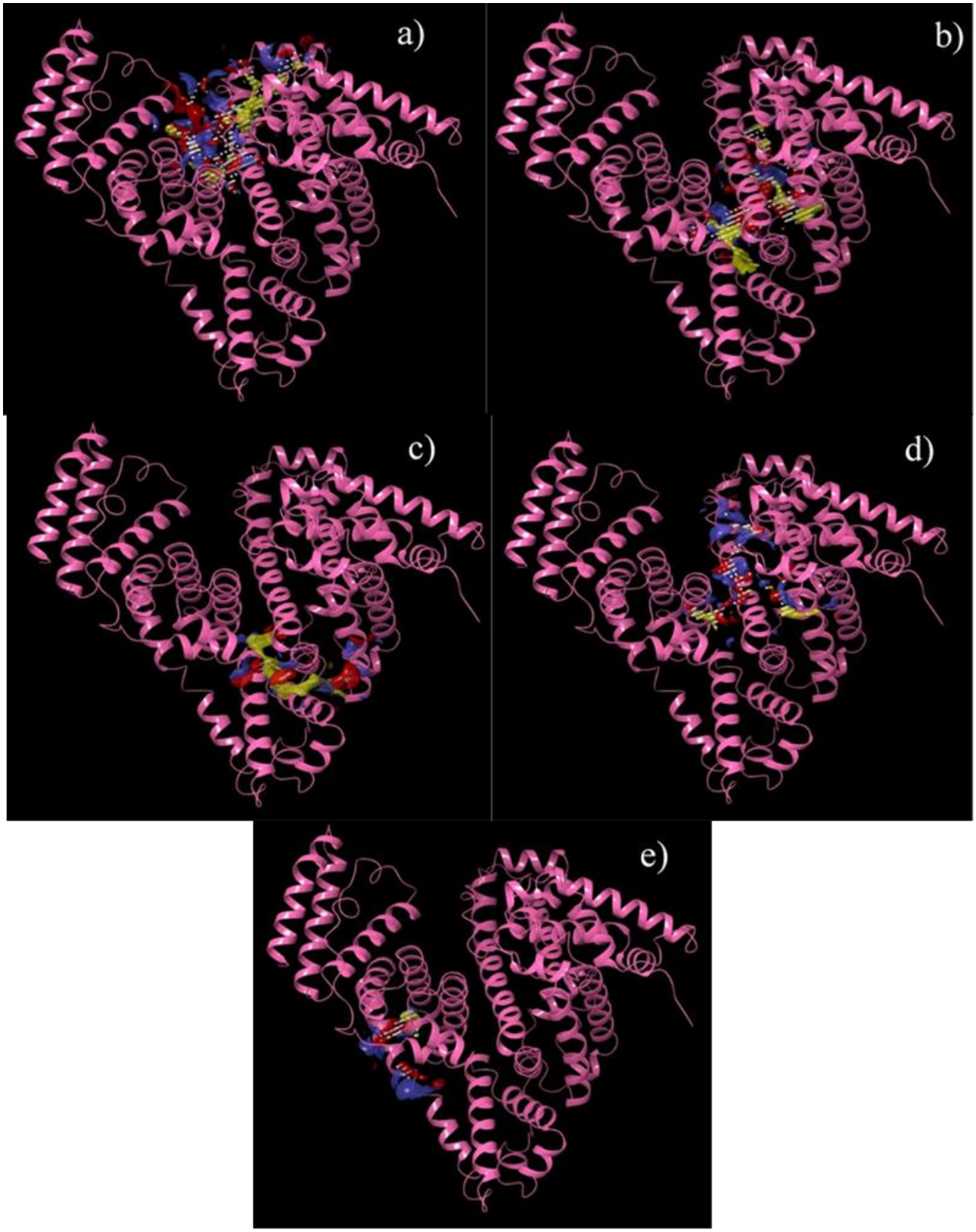

Figure S33: Binding site determination in **BSA**: The likely binding sites were identified using the SiteMap application in Maestro. The red, blue, and yellow regions marked in the protein **BSA** indicate ligand acceptor, ligand donor, and hydrophobic sites, respectively.

Table S10: Tabulated gist of the docking calculations at different sites in **BSA**. The docking score reveals the binding affinity for the best-docked poses in each case.

PDB ID and Site	Interacting amino acids	Docking Score (kcal/mol)	Types of interactions
4F5S Site 1	Pro 110, Ser 109, Asp 108, Arg 196, Arg 144, His 145, Pro 146, Tyr 147, Val 461, Ala 193, Ser 192, Thr 190, Arg 458, Ile 455, Leu 189, Leu 454, Tyr 451, Arg 435, and Ser 428	-5.399	Hydrophobic interactions with Tyr 451, Leu 454, Ile 455, Leu 189, Val 461, Leu 189, Ala 193, Tyr 147, Pro 146 and Pro 110. Polar interaction with Ser 109, His 145 and Ser 428. Positive charged interactions with Arg 435, Arg 458, Arg 144 and Arg 196. Negative charge interaction with Asp 108.
Site 2	Glu 152, Tyr 149, Arg 198, Arg 217, Arg 194, Ser 191, Hie 241, Ile 263, Ala 260, Leu 259, Arg 256, Leu 233, Leu 237, Phe 222, Lys 221, Leu 218, Glu 291, Ala 290, Ile 289, Lys 221, Trp 213	-4.487	Hydrophobic interactions with Tyr 149, Leu 218, Trp 213, Ala 290, Ile 289, Phe 222, Leu 233, Leu 259, Ala 260, Ile 263, Leu 237. Positively charged interaction with Arg 194, Arg 198, Arg 217, Lys 221 and Arg 256. Negatively charged interactions with Glu 291 and Glu 152. Polar interactions with Hie 241 and Ser 191
Site 3	Lys 350, Ser 479, Leu 480, Val 481, Leu 346, Ala 212, Ala 209, Arg 208, Lys 204, Phe 205, Gly 206	-4.013	Hydrophobic interactions with Leu 346, Val 481, Leu 480, Ala 212, Ala 209, Phe 205. Hydrogen bonding with Arg 208. Positive charged interaction with Lys 350 and Lys 204. Polar interactions with Ser 479.
Site 4	Lys 204, Lys 465, Hip 105, Lys 106, Arg 196, Asp 108, Asp 107, Glu 464, Ser 104, Tyr 147 and Tyr 84	-3.211	Charged (negative) interaction with Asp 108, Asp 107, Glu 464. H-bond interaction with Lys 204. Cation-Pi interaction with Lys 465. Polar interactions with Ser 104. Hydrophobic interactions with Tyr 147, Tyr 84.
Site 5	Leu 386, Asn 390, Leu 429, Leu 452, Leu 456, Leu 406, Arg 484, Arg 309, Tyr 410, Phe 487, Ser 488, Lys 413, Leu 490, Thr 491 and Pro 492	-2.333	Hydrophobic interactions with Leu 386, Leu 429, Leu 452, Leu 456, Leu 406, Tyr 410, Phe 487, Leu 490, Pro 492. Polar interactions with Thr 491, Ser 488, Asn 390. Positive charged interactions with Arg 484, Arg 409 and Lys 413

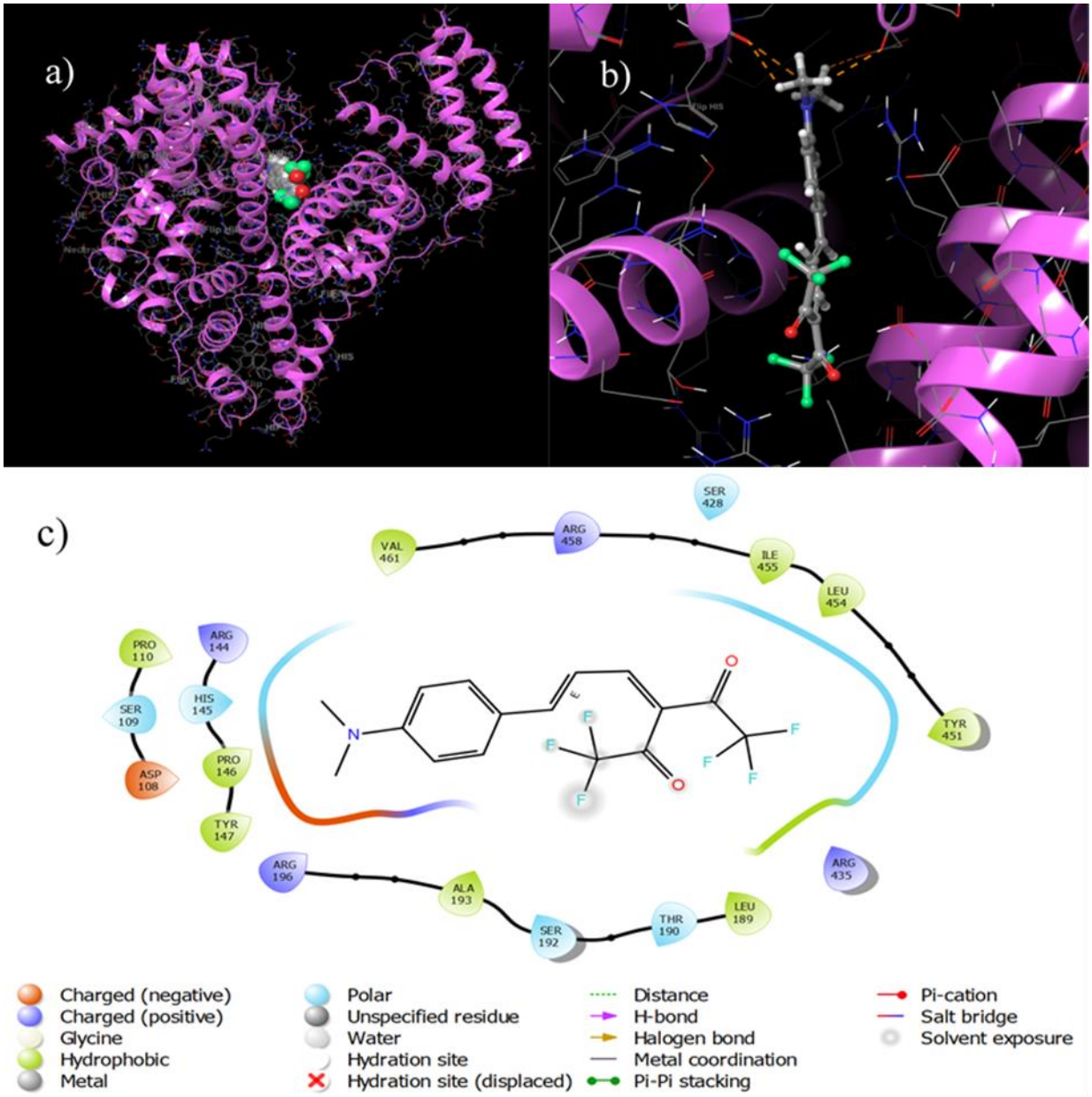

Figure S34: Binding interaction between A4 and site 1 of 4F5S. **a)** Shows the location of A4 in the protein. **b)** It shows the zoomed-in view of the A4 interaction with **BSA**. **c)** Lig-plot corresponding to the interaction between A4 and amino acids of the site 1 of 4F5S.

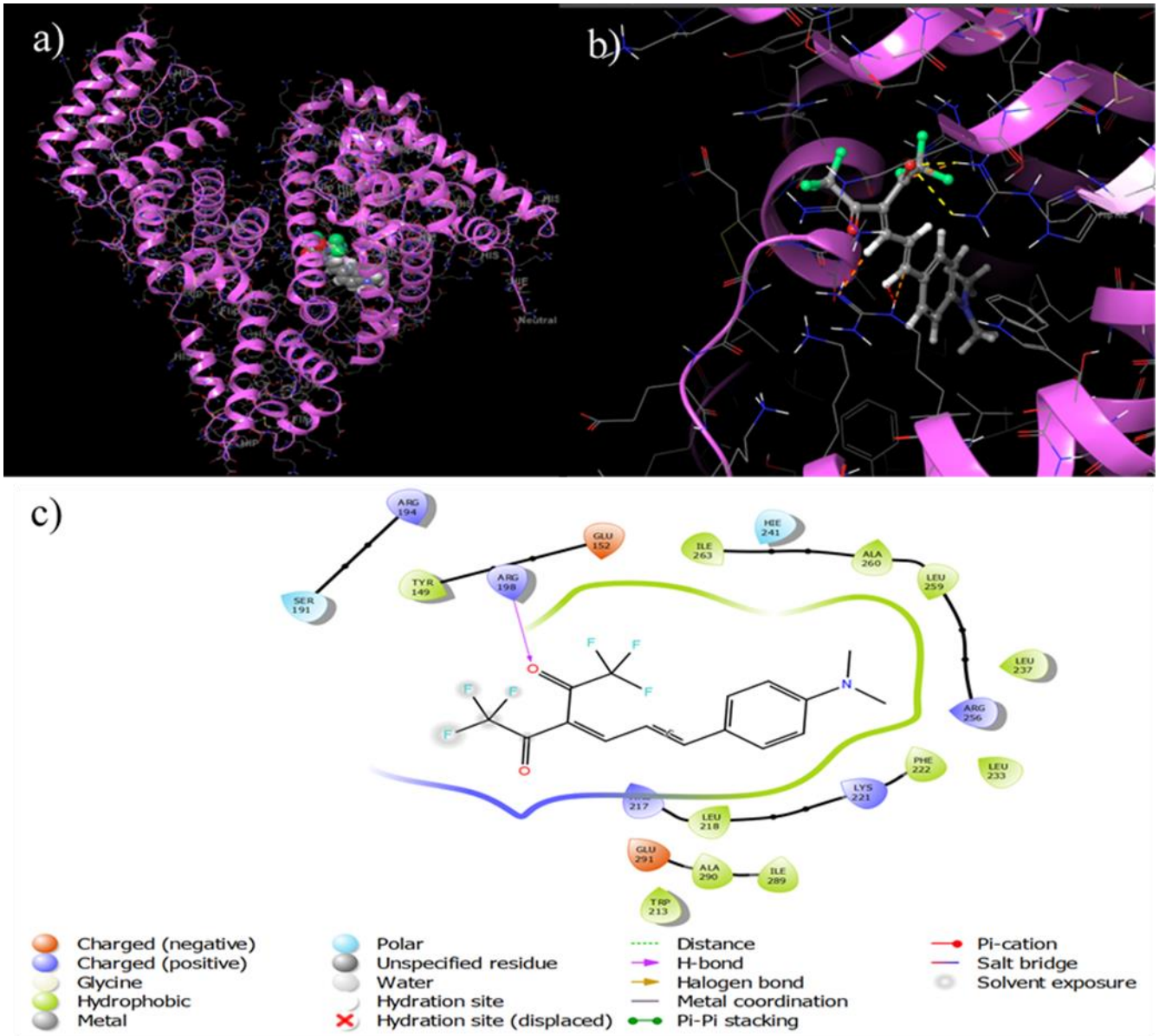

Figure S35: Binding interaction between A4 and site 2 of 4F5S. **a)** Shows the location of A4 in the protein. **b)** It shows the zoomed-in view of the A4 interaction with **BSA**. **c)** Lig-plot corresponding to the interaction between A4 and amino acids of the site 2 of 4F5S.

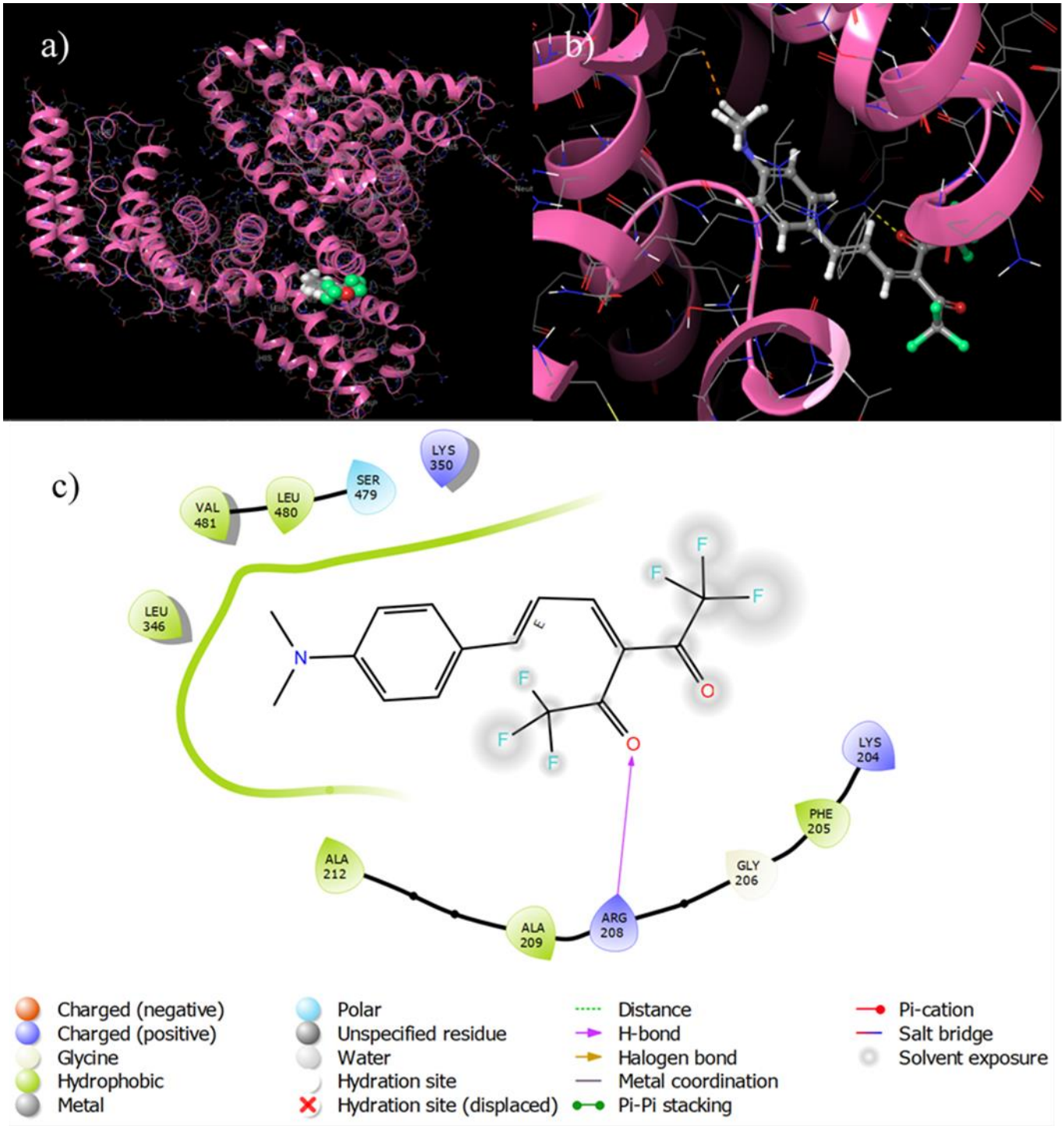

Figure S36: Binding interaction between A4 and site 3 of 4F5S. **a)** Shows the location of A4 in the protein. **b)** It shows the zoomed-in view of the A4 interaction with **BSA**. **c)** Lig-plot corresponding to the interaction between A4 and amino acids of the site 3 of 4F5S.

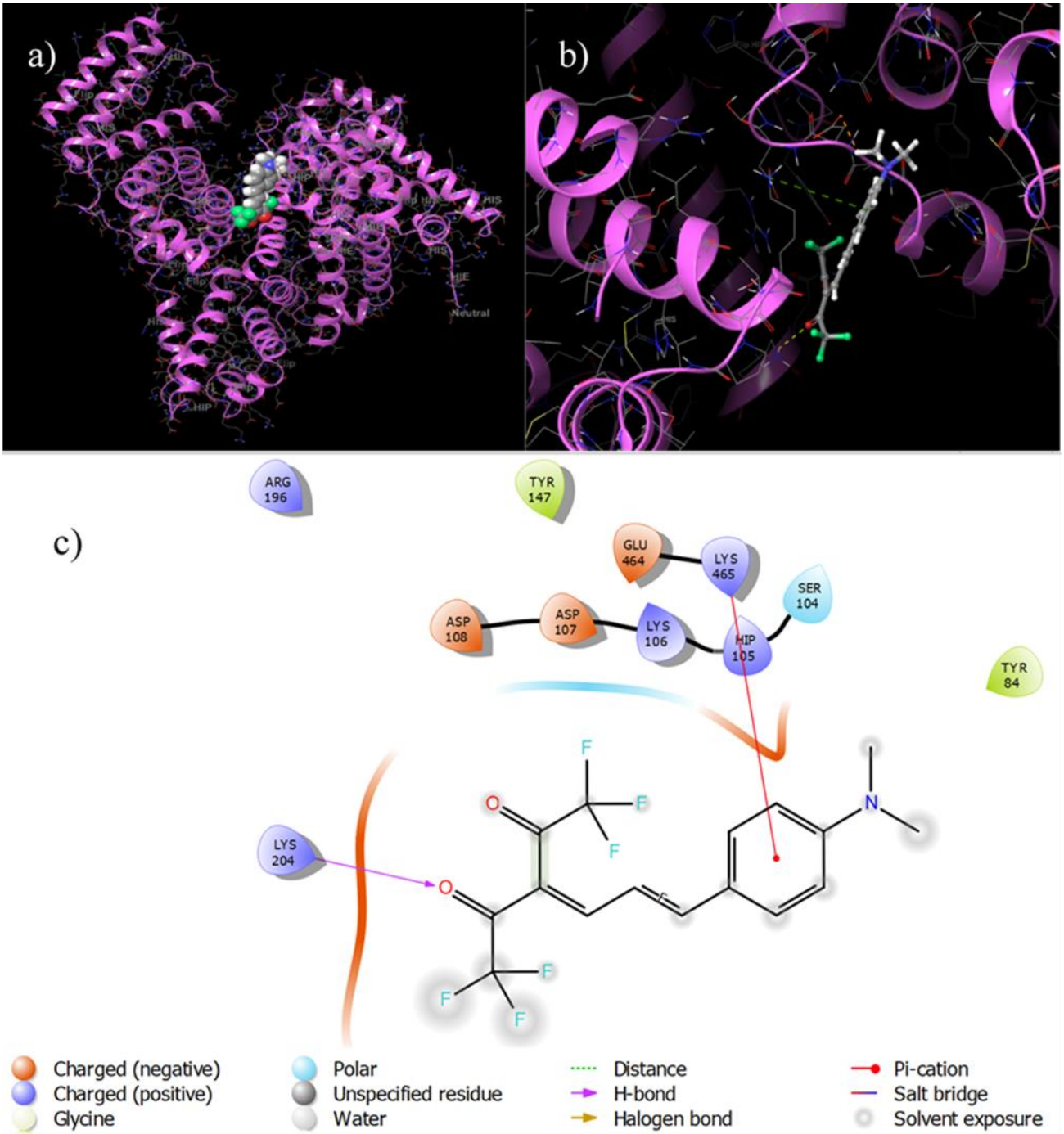

Figure S37: Binding interaction between A4 and site 4 of 4F5S. **a)** Shows the location of A4 in the protein. **b)** It shows the zoomed-in view of the A4 interaction with **BSA**. **c)** Lig-plot corresponding to the interaction between A4 and amino acids of the site 4 of 4F5S.

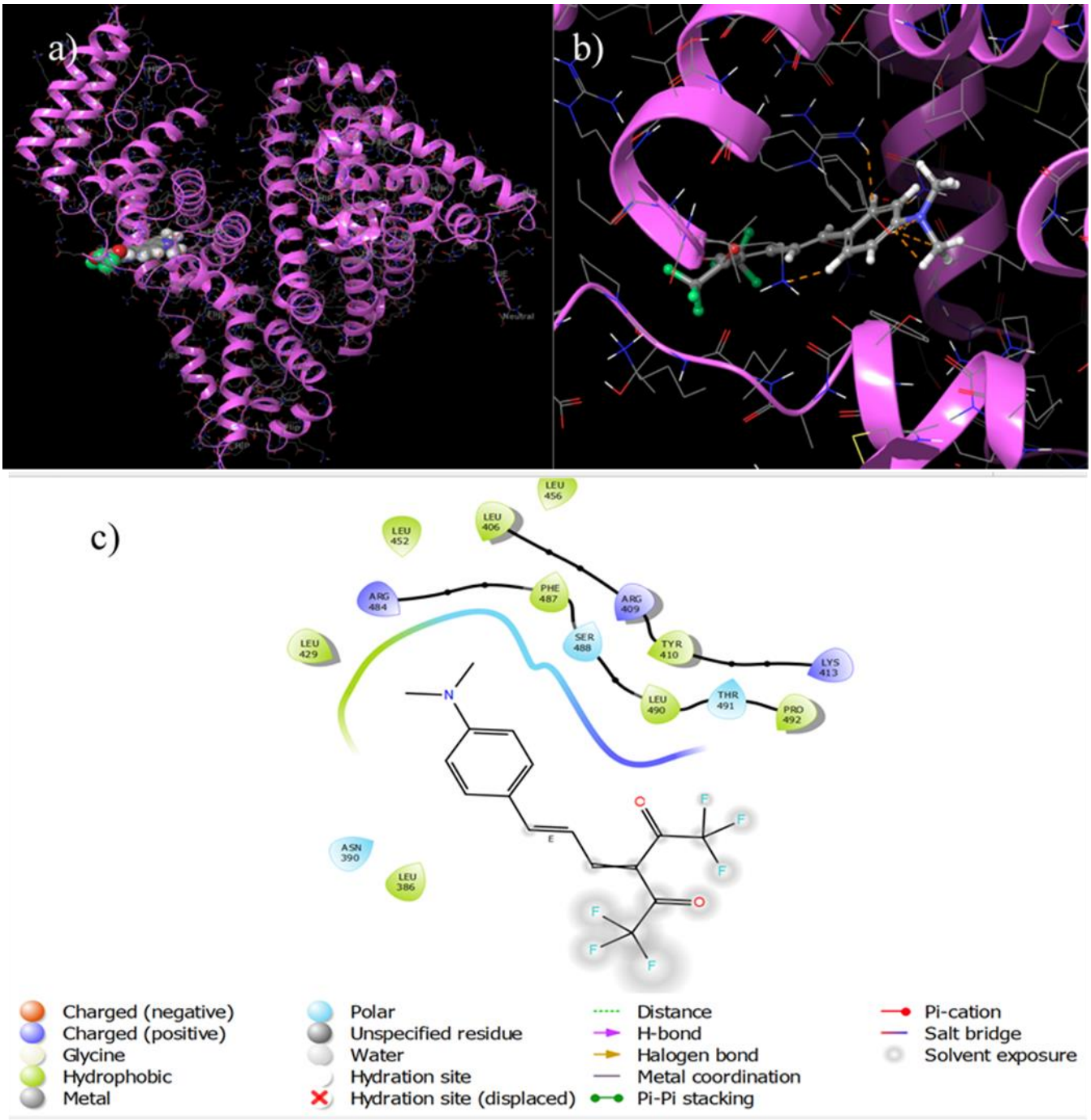

Figure S38: Binding interaction between A4 and site 5 of 4F5S. **a)** Shows the location of A4 in the protein. **b)** It shows the zoomed-in view of the A4 interaction with **BSA**. **c)** Lig-plot corresponding to the interaction between A4 and amino acids of the site 5 of 4F5S.

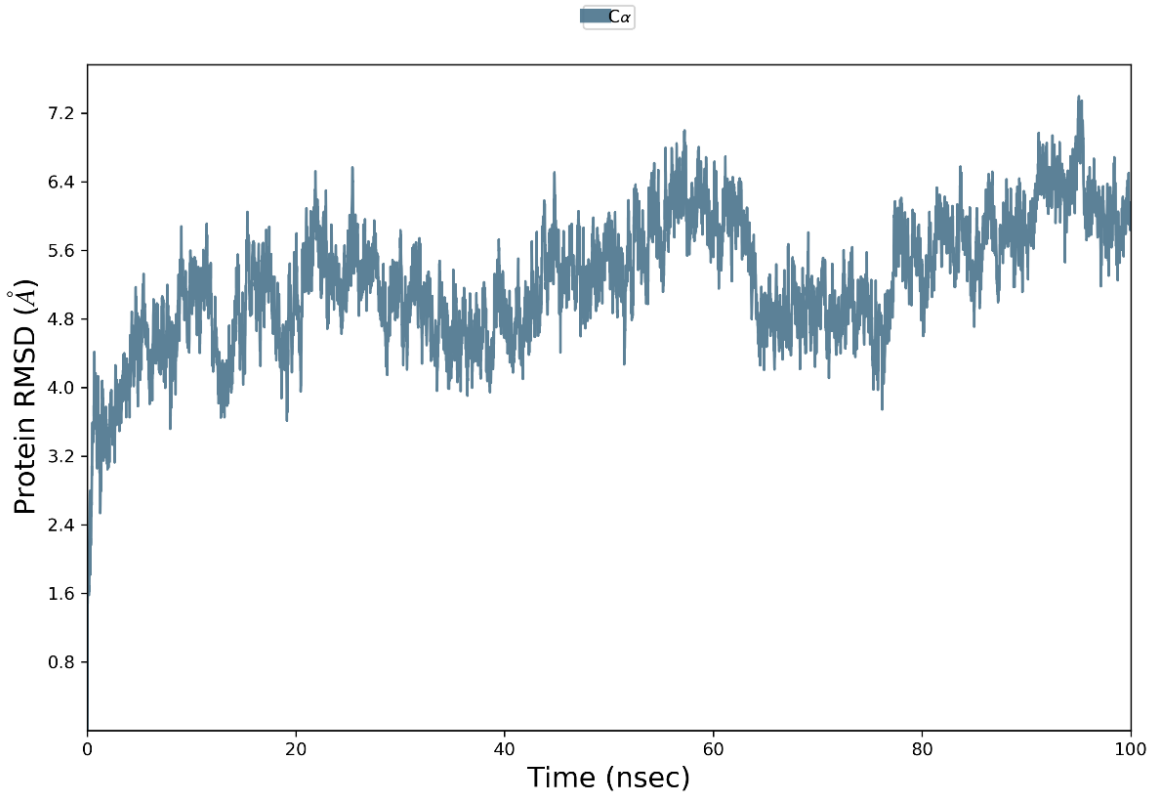

Figure S39: The RMSD plot obtained for the free HSA. The protein C_α is shown in blue colour.

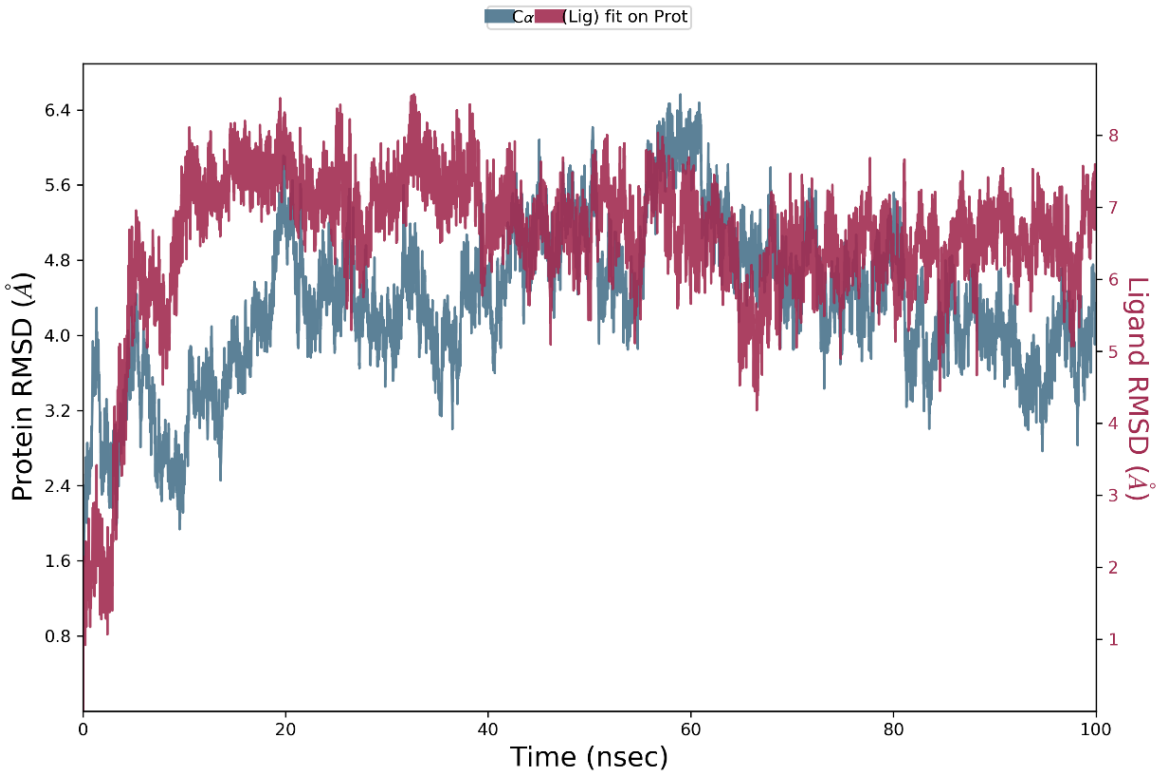

Figure S40: The RMSD plot obtained for the HSA-A4 ensemble. The protein C_α and the probe A4 are shown in blue and red colours, respectively.

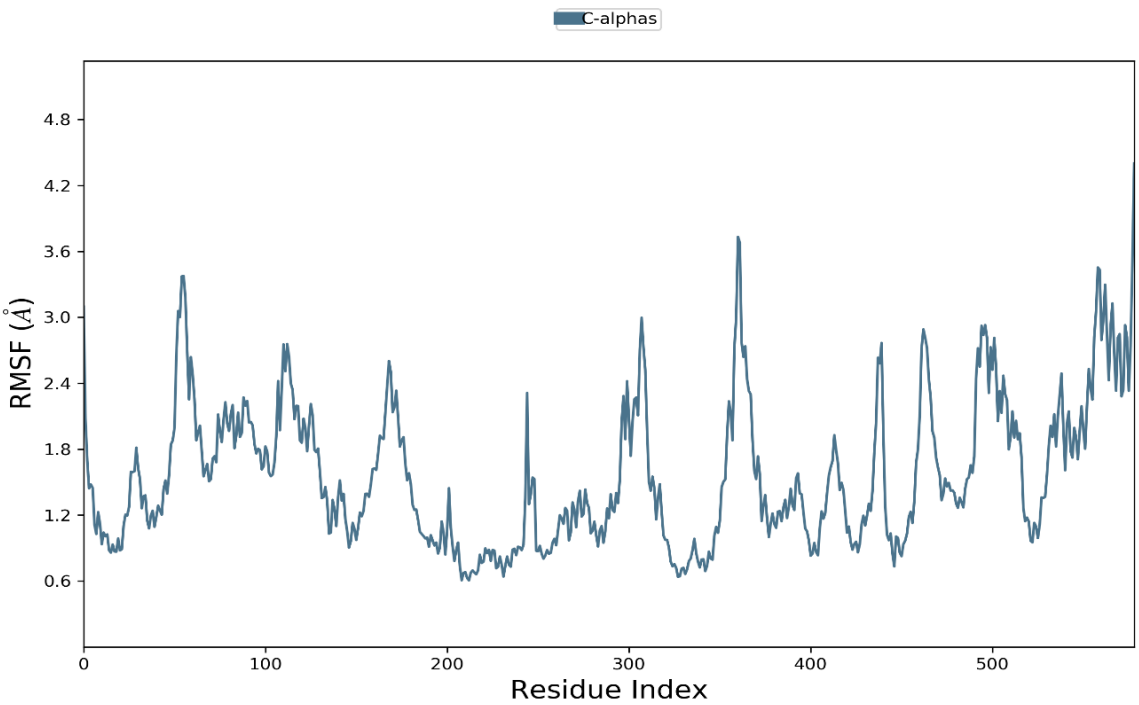

Figure S41: The RMSF plot of the apo protein's (HSA alone) backbone atoms during the 100 ns MD Simulations. The protein C_α is shown in blue.

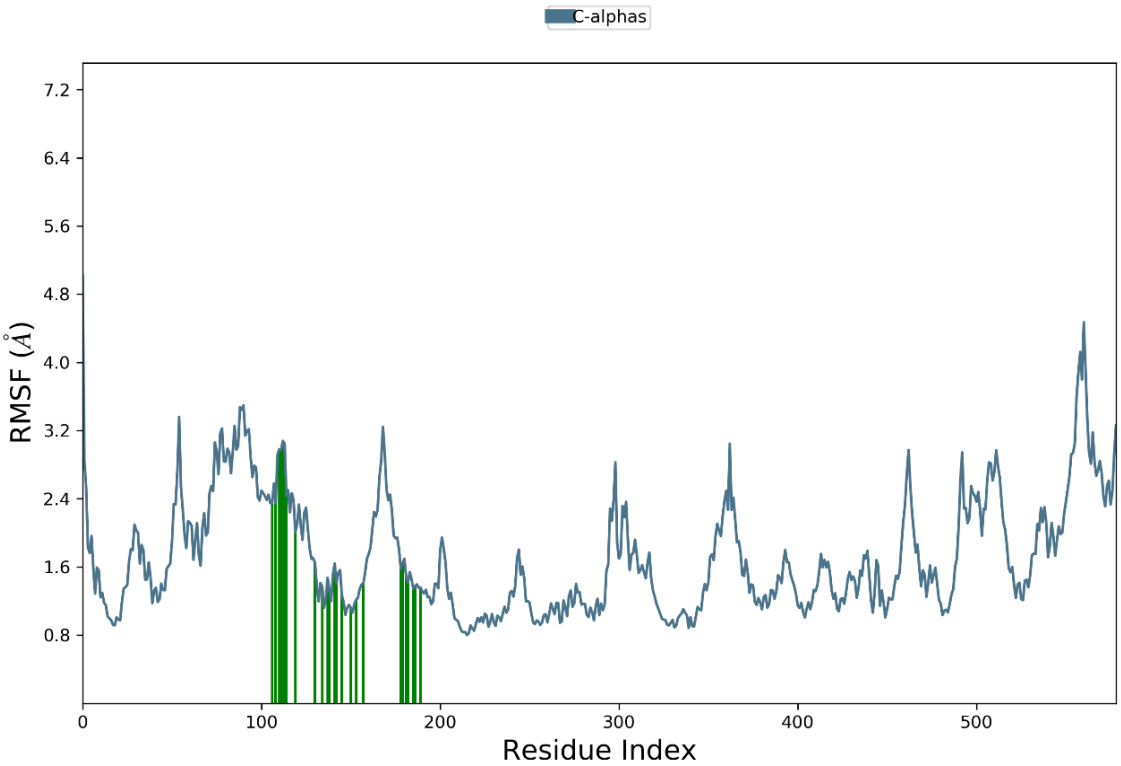

Figure S42: The RMSF plot of the protein's (A4-HSA) backbone atoms during the 100 ns MD Simulations. The protein C_α is shown in blue.

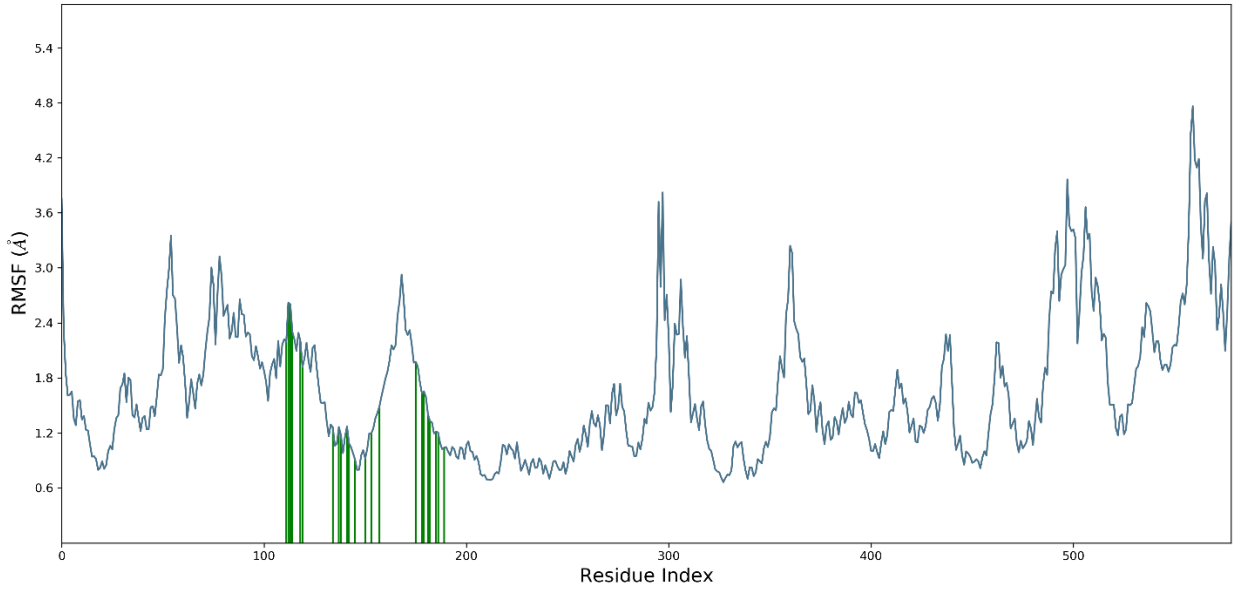

Figure S43: The RMSF plot of the protein's (A4*-HSA) backbone atoms during the 100 ns

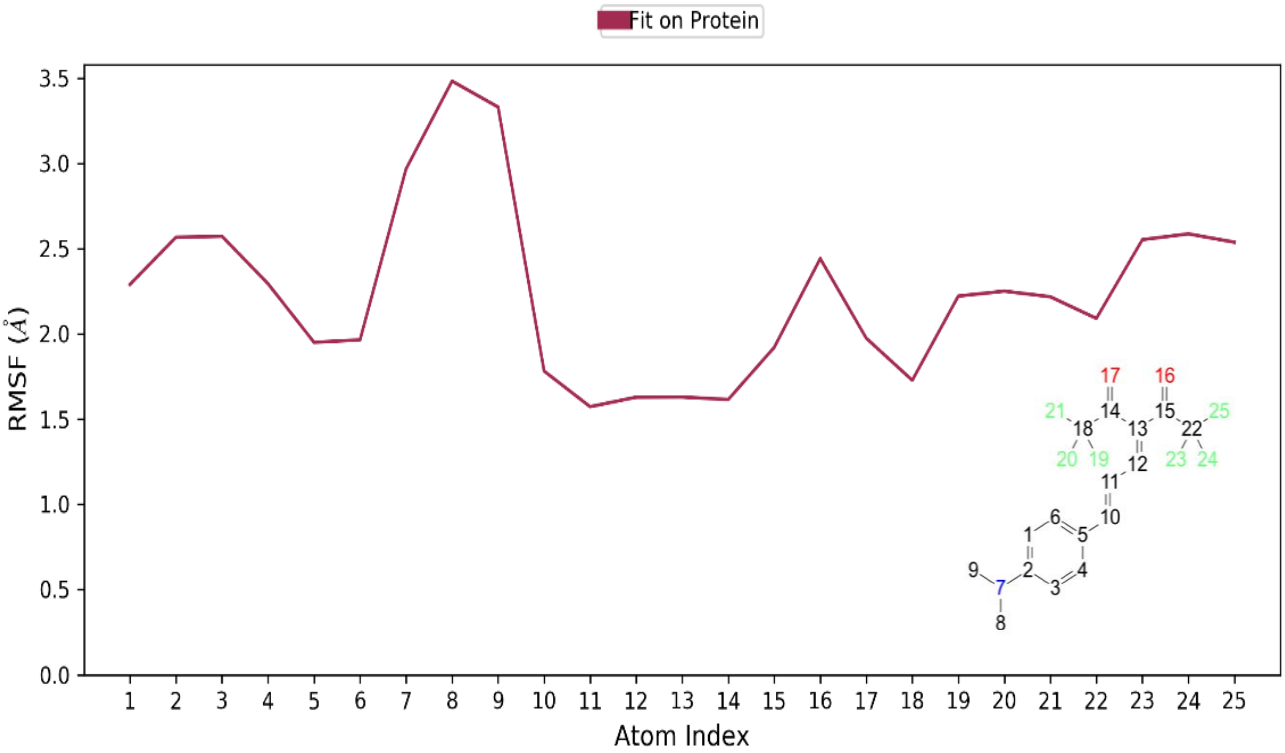

Figure S44: The RMSF plot of the ligand A4 atoms inside the protein pocket during the 100 ns MD Simulations.

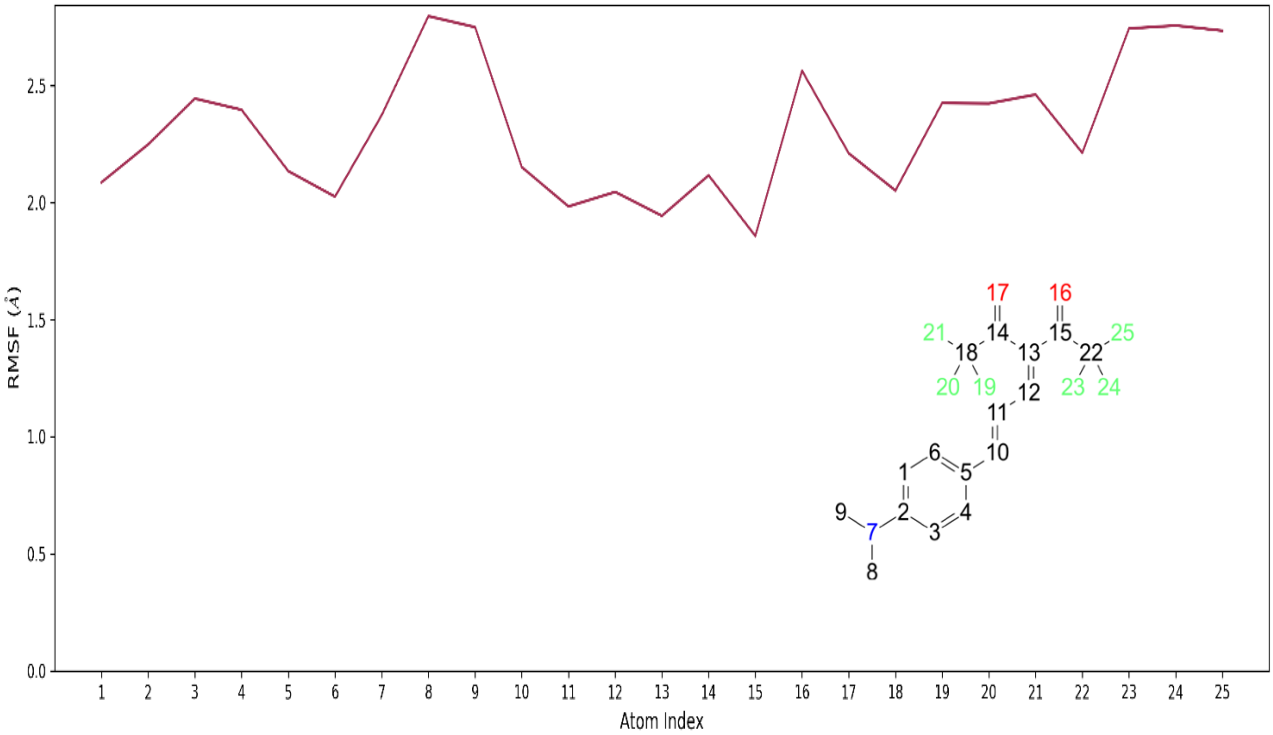

Figure S45: The RMSF plot of the ligand A4* atoms inside the protein pocket during the 100ns M D Simulations.

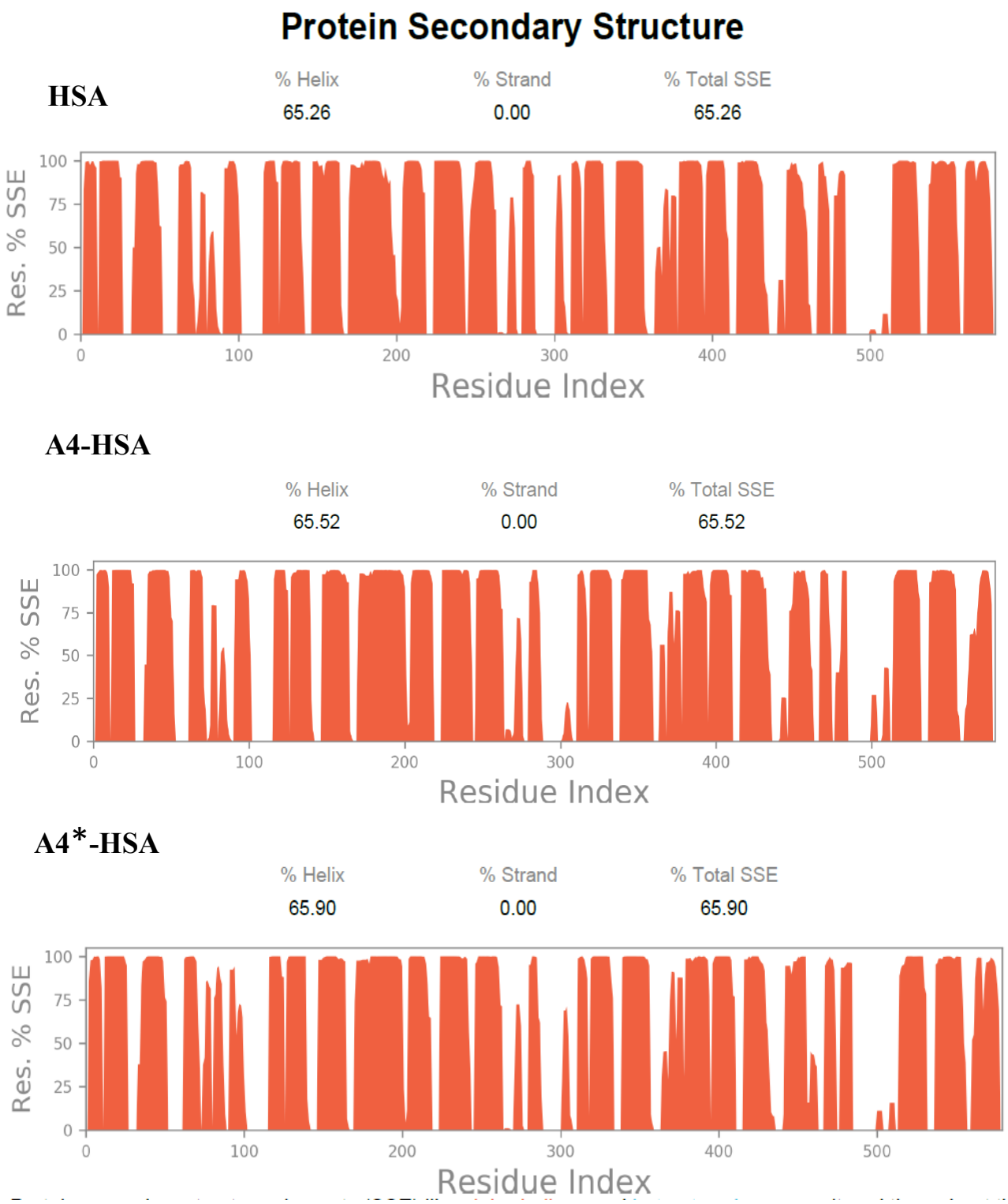

Figure S46: The protein secondary structure elements (SSE) were monitored throughout the simulation the plot represents SSE distribution by residue index for the entire protein structure. Orange color is used to denote α- helices.

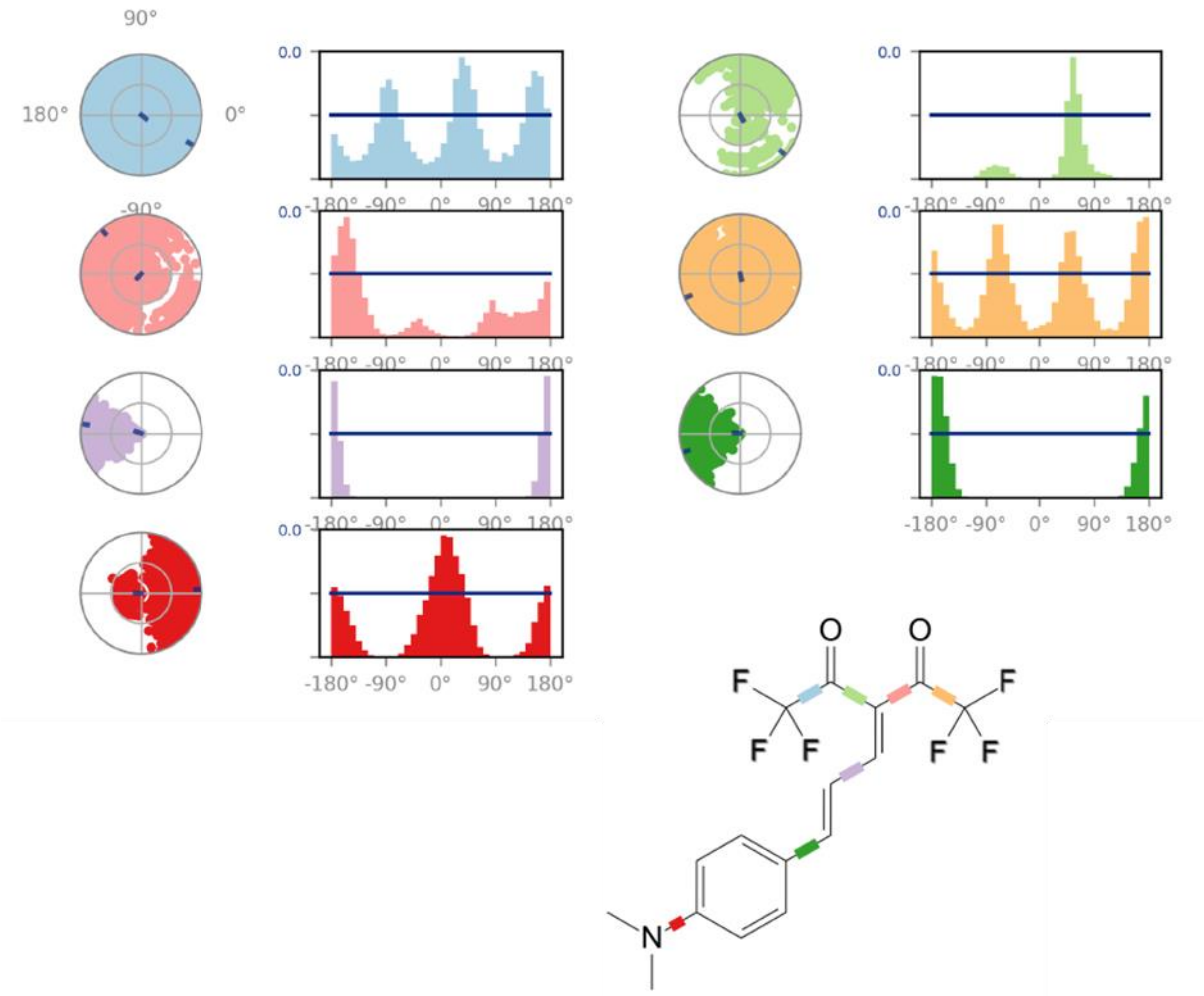

Figure S47: A4 ligand torsion plots inside the protein pocket.

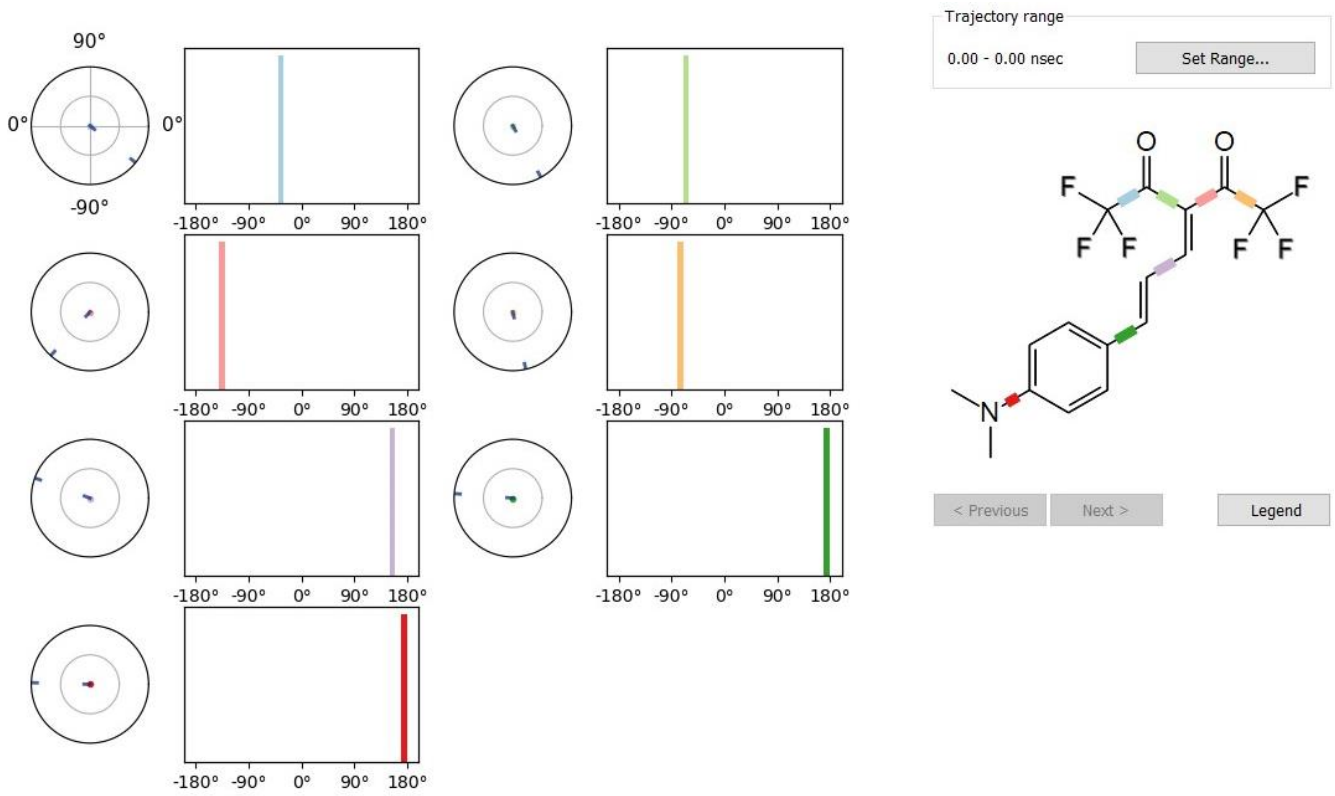

Figure S48: A4 ligand torsion plots inside the protein pocket at time t=0.

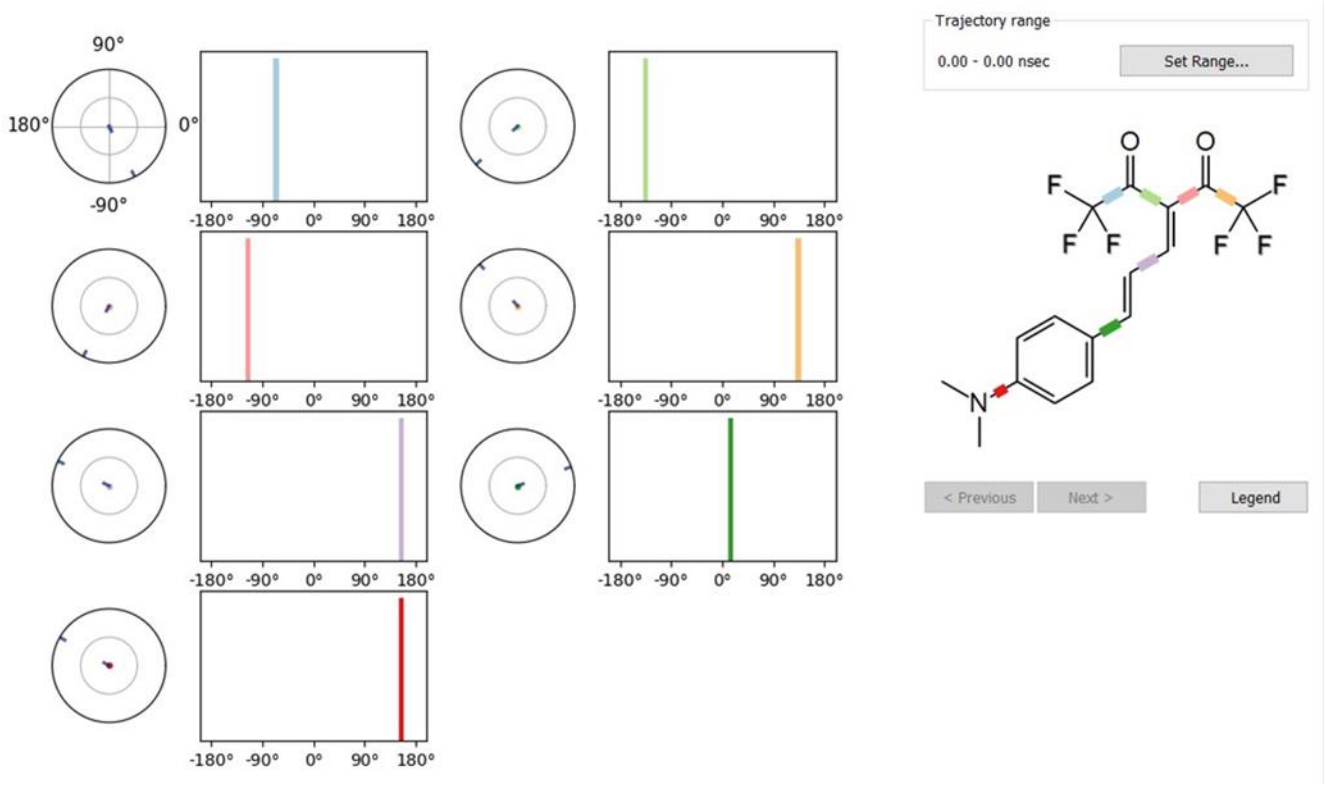

Figure S49: A4* ligand torsion plots inside the protein pocket at time t=0.

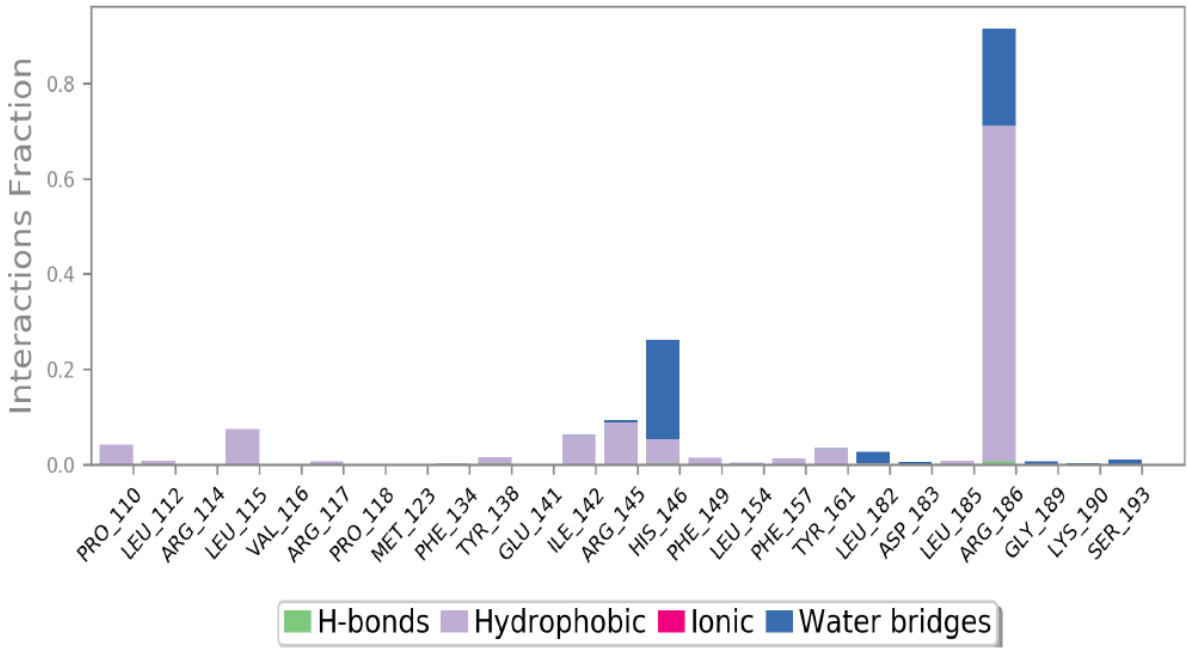

Figure S50: Histogram representing protein residues interacting with ligand A4 in each trajectory frame during the simulation. Interaction fraction summary of 1O9X-A4 contacts. The bar plots are normalized over the entire course of the trajectory. Say a value of 0.2 against a particular amino acid in such a plot suggests that the ligand maintains contact with that amino acid for 20% of the simulation time. While a value over 1.0 suggests that a specific amino acid residue makes multiple contacts of the same kind with the ligand. This histogram represents the protein residues interacting with ligand A4 in each trajectory frame during the simulation. Lilac color stands for hydrophobic interactions; blue color stands for water bridges.

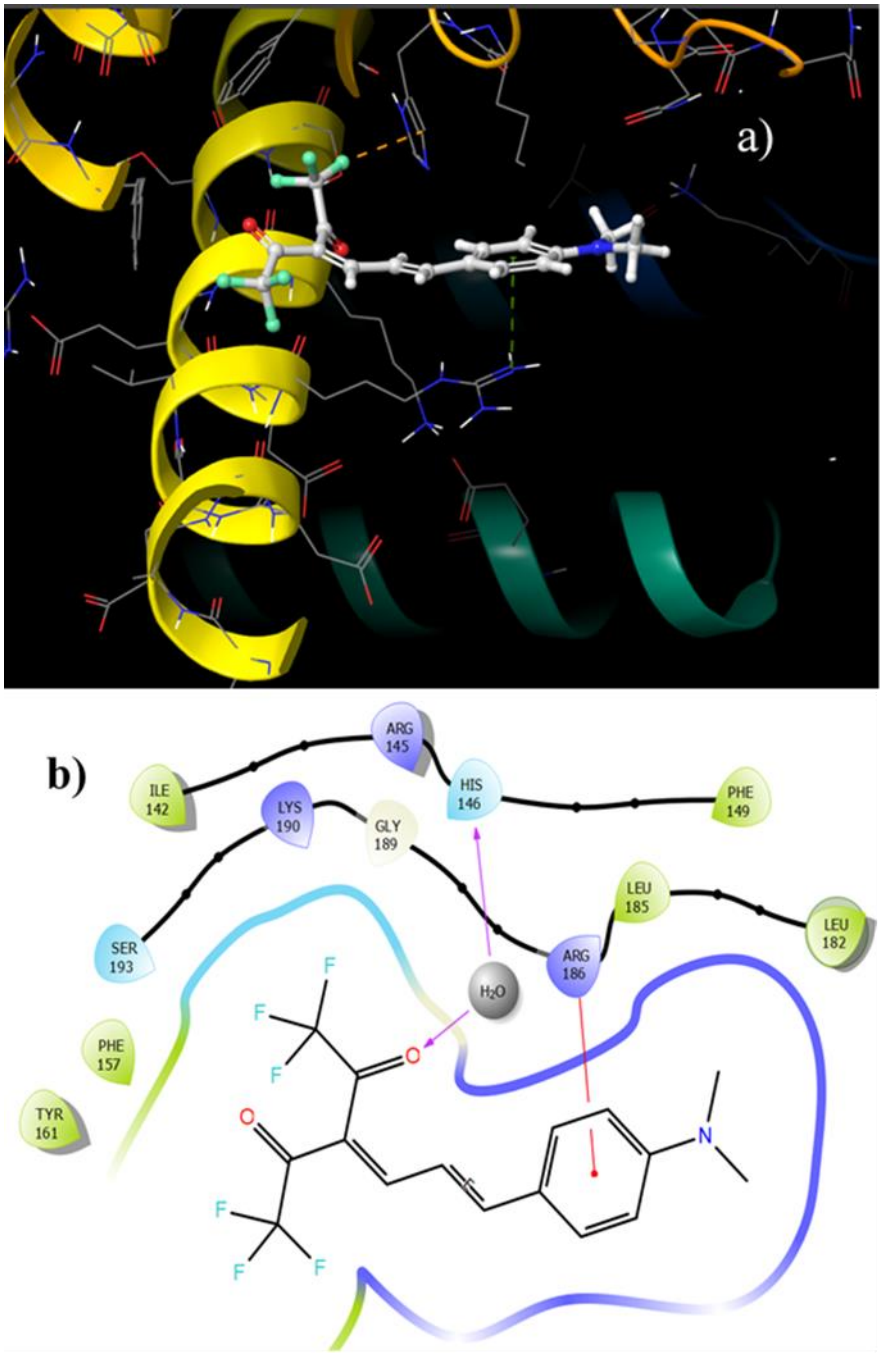

Figure S51: Snapshot of a trajectory frame showing HSA –A4 interaction (a) and its corresponding ligand plot (b).

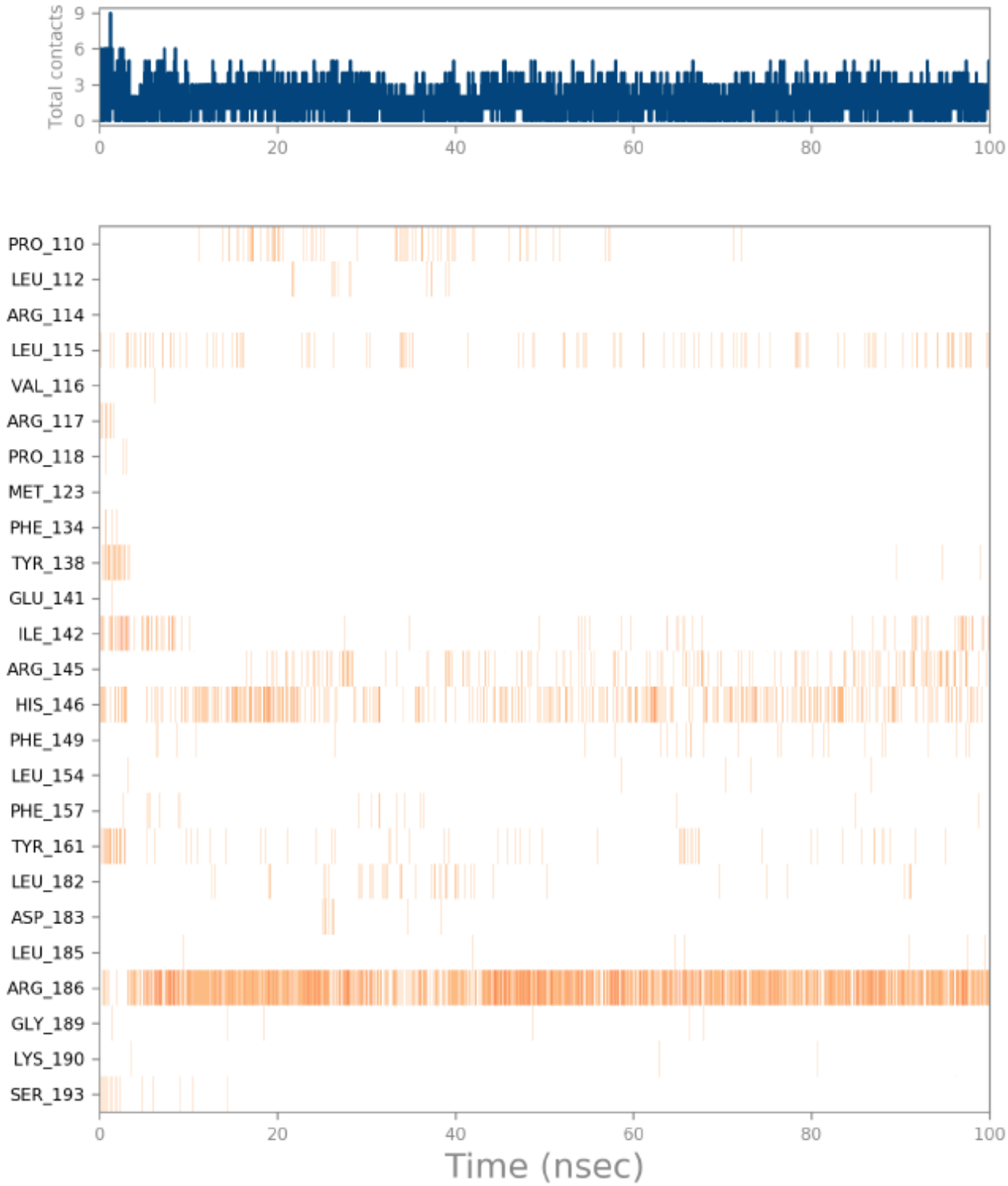

Figure S52: The protein-ligand contact plot showing the time points where the protein residues interact with ligand A4 during the simulation. Protein-ligand contacts showing good contacts (darker shade of orange) with the amino acid residue **Arg 186** over 100ns time period of simulation.

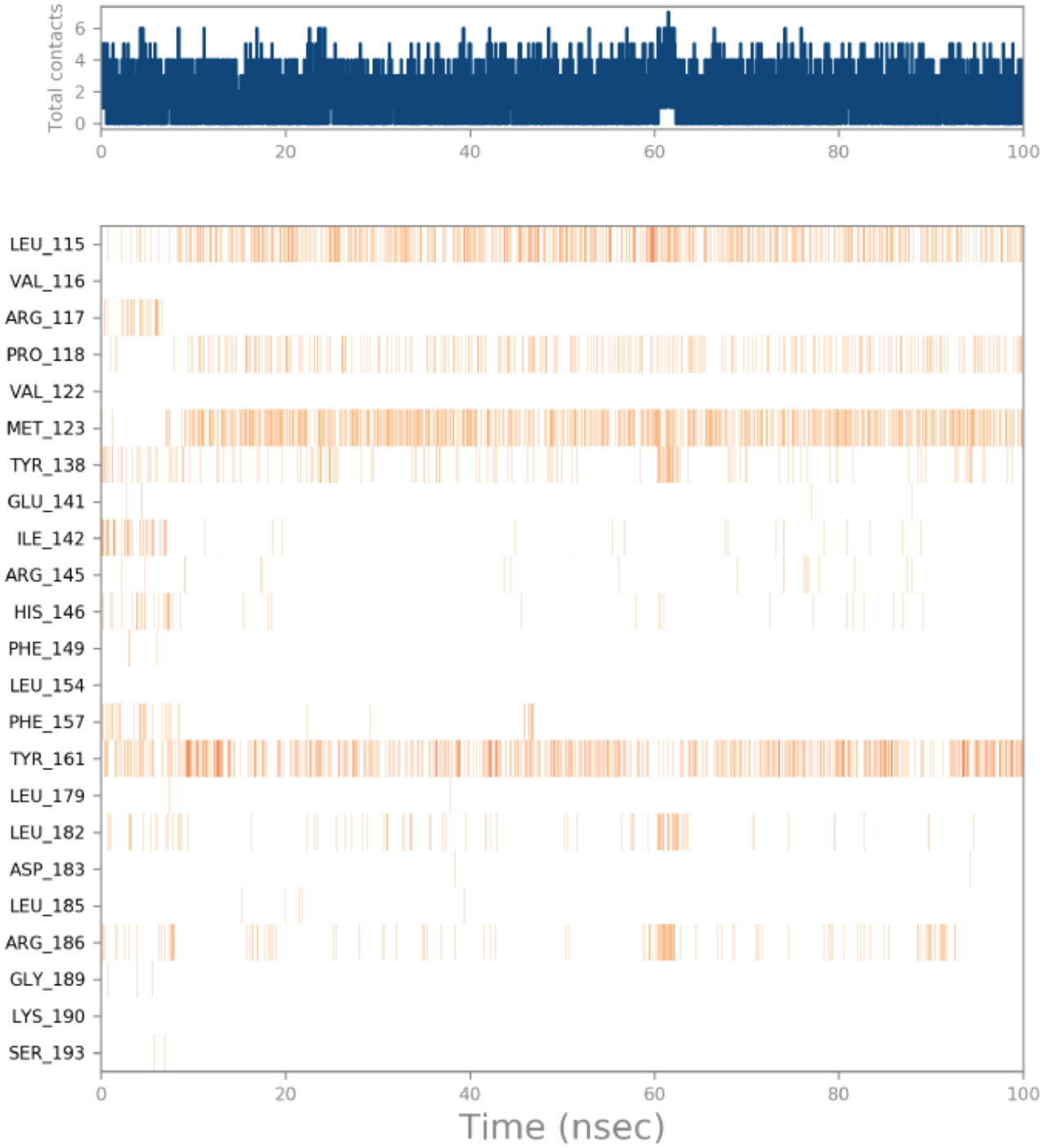

Figure S53: The protein-ligand contact plot showing the time points where the protein residues interact with ligand A4* during the simulation.

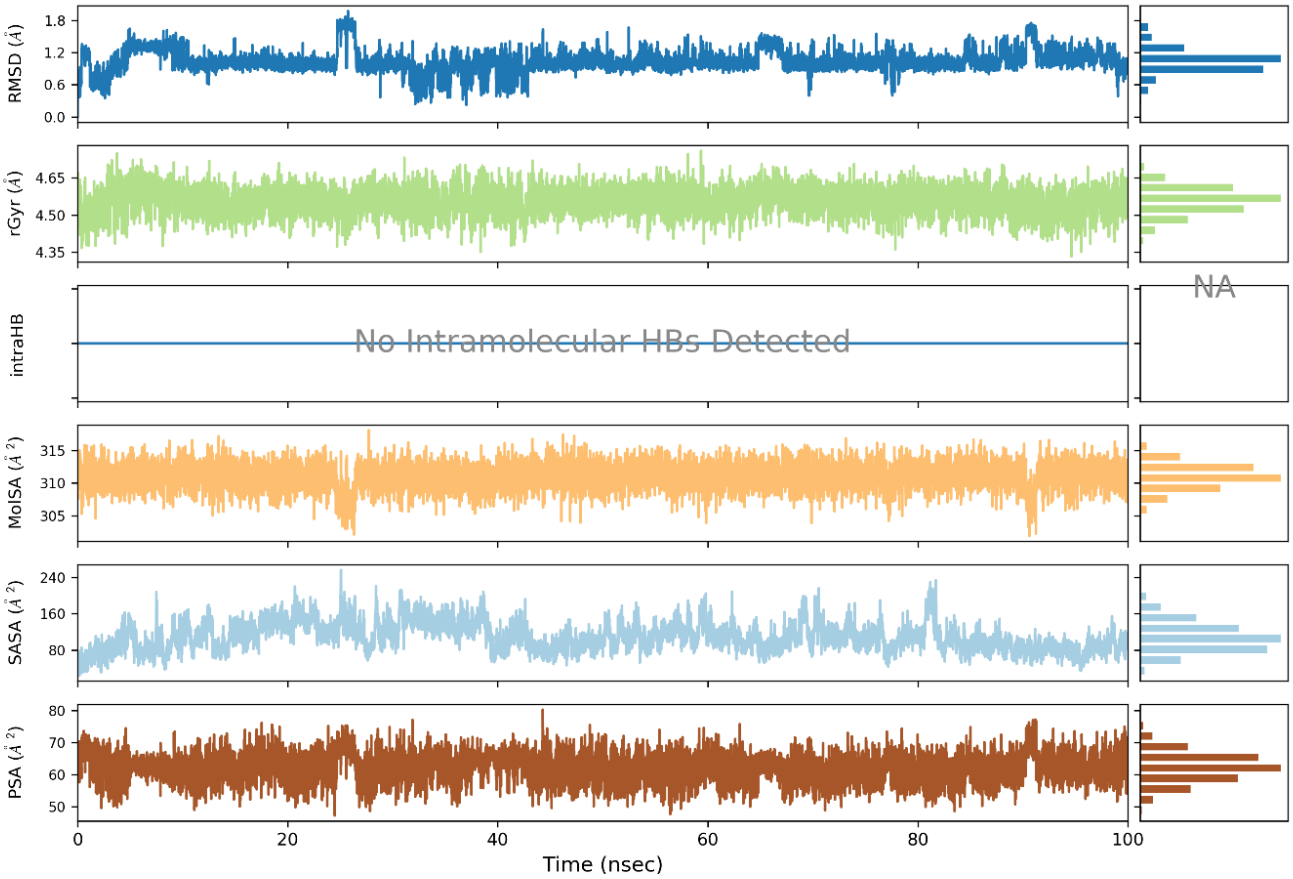

Figure S54: The ligand property trajectory of A4 in the A4-HSA ensemble during the course of the simulation. These include the radius of gyration (rGyr), intramolecular H-bonding (if any), solvent-accessible surface area (SASA), the molecular surface area of ligand (MolSA), and polar surface area (PSA).

Note: Simulation trajectory videos will be made available on request.

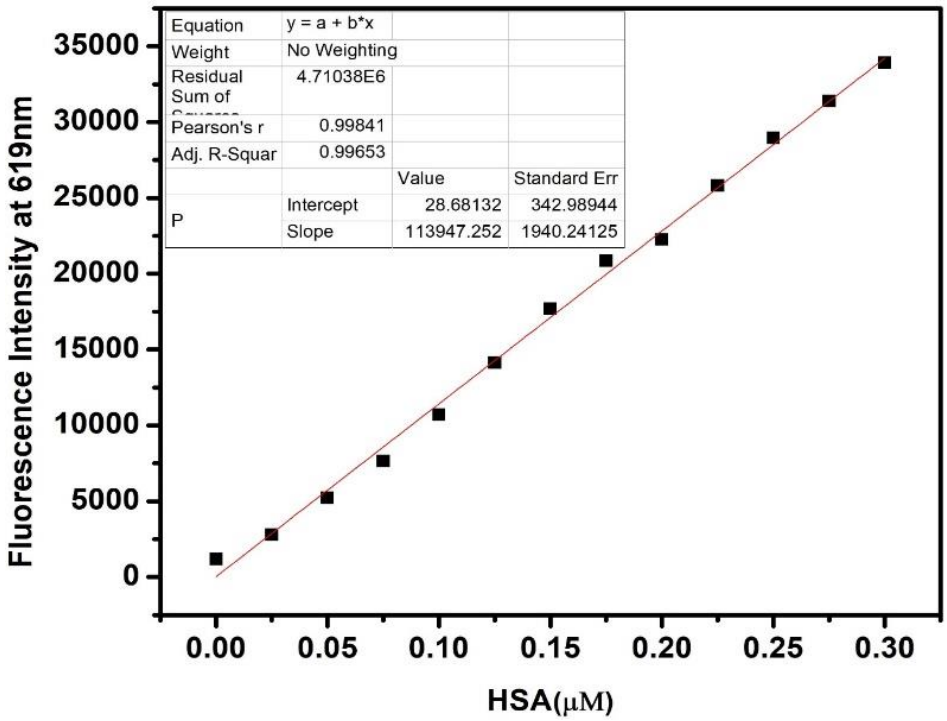

Figure S55: The titration plot of one of the experiments shows an excellent linearity marked by the R^2 value of 0.99. The change in emission intensity of A4 upon the addition of a 10-fold diluted urine sample in PBS.

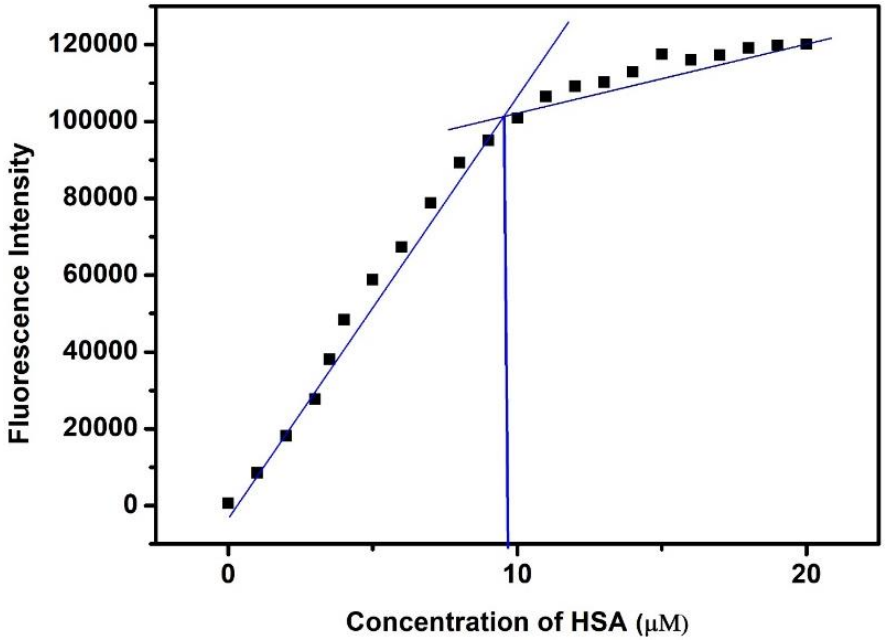

Figure S56: Determination of binding stoichiometry of A4 (10μM) and HSA (10μM) using the change in fluorescence intensity of A4 upon increasing addition of HSA. A4 and HSA bind in a 1:1 stoichiometry.

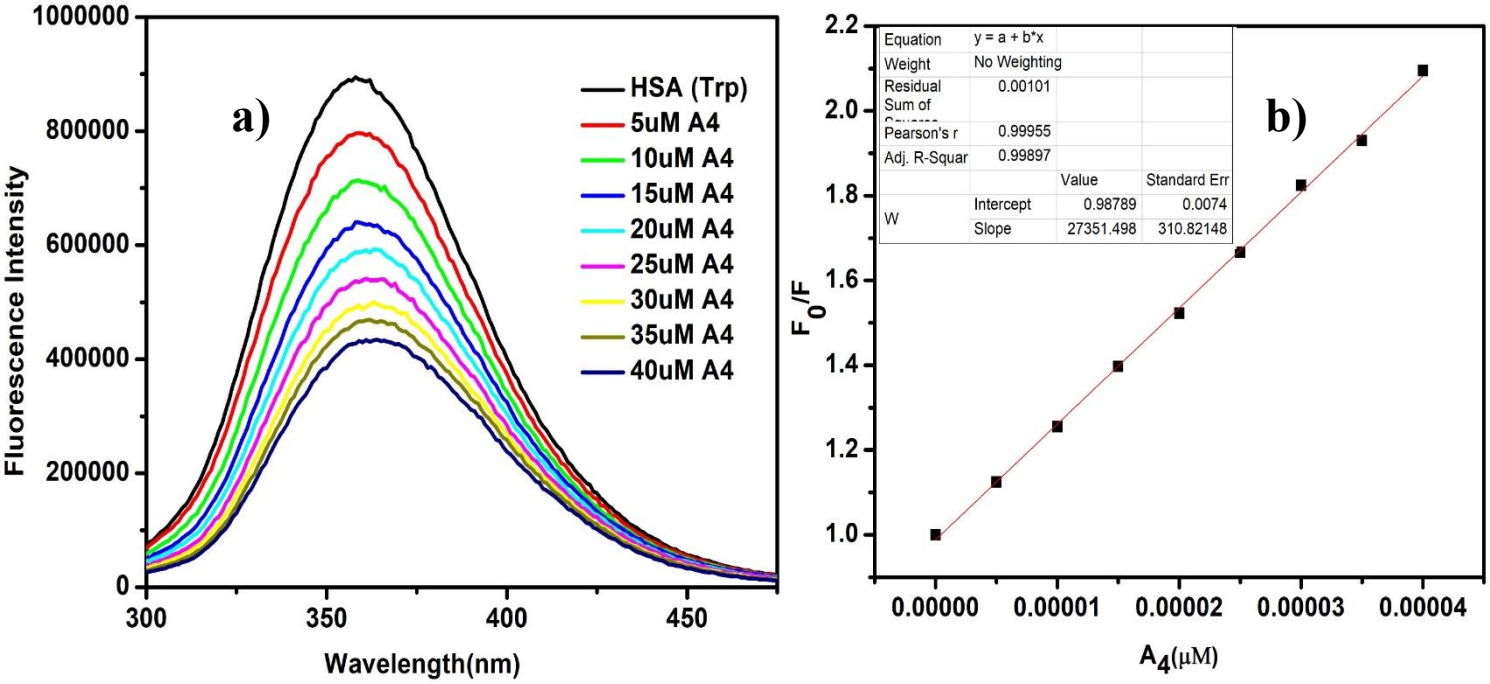

Figure S57: a) The fluorescence quenching plot of HSA where ligand A4 acts as the quencher.

b) Stern Volmer plot for fluorescence quenching with increasing concentrations of A4.

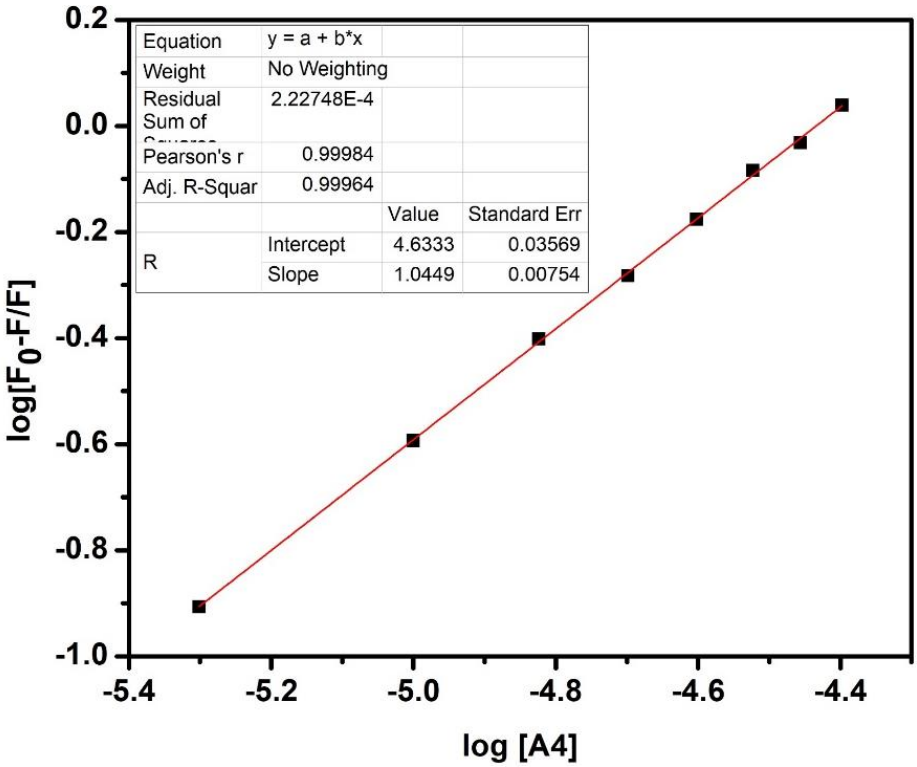

Figure S58: Double logarithmic plot (the Modified Stern Volmer plot) for HSA and A4.

The modified Stern Volmer equation is: $\log [F_0\text{-}F/F] = \log K_b + n \log [Q]$,

Where F_0 = the initial fluorescence intensity

F= fluorescence intensity values upon addition of the quencher

K_b =the binding constant

n =slope of the curve=the number of binding sites= 1 (here)

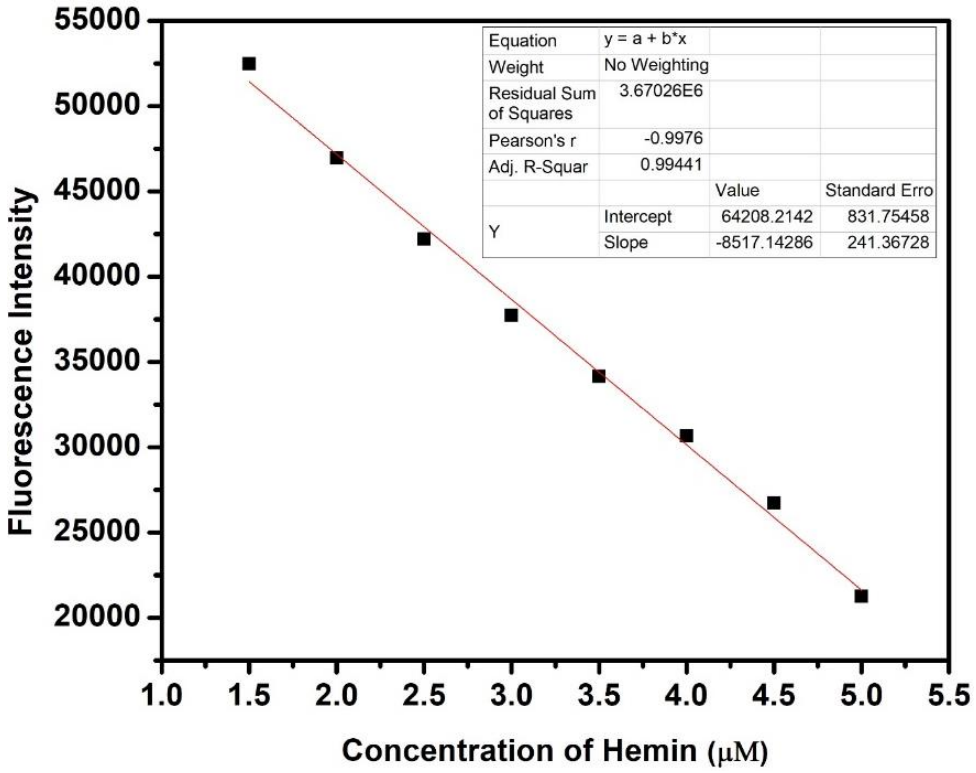

Figure S59: The Calibration curve at λem= 619nm for calculating the detection limit of Hemin using HSA-A4. The limit of detection and the limit of quantitation were calculated using the formulae 3σ/S and 10σ/S.

Table S11: A table of comparison between the probes reported for hemin and work.

Probe	**Technique used**	**Limit of Detection**	**Reference**
CdS QDs/protamine	Fluorescence	48.6 nM	20
Luminol/Artemisinin	Chemiluminescence	0.37 nM	21
Artemisinin-thiamine	Fluorescence	0.68 nM	22
Rhodamine B/H2O2/NaOH	Chemiluminescence	0.086 nM	23
Acridine Orange-PS2.M/rGO	Fluorescence	50 nM	24

H_2O_2, TBHP, Artemisinin/ dihydrofluorescein	Fluorescence	0.064/0.35/0.42 nM	25
Carboxylate graphene / Hemin-binding-aptamer (HBA) nanocomposite	Square wave voltammetry	0.64nM	26
(Dicyanomethylene-4H-pyrans-morpholine**) DCM-ML**/HSA	Fluorescence	9-15nM	27
Curcumin Polymer	Fluorescence	13.5μM	28
This work	Fluorescence	0.23 μM	This work

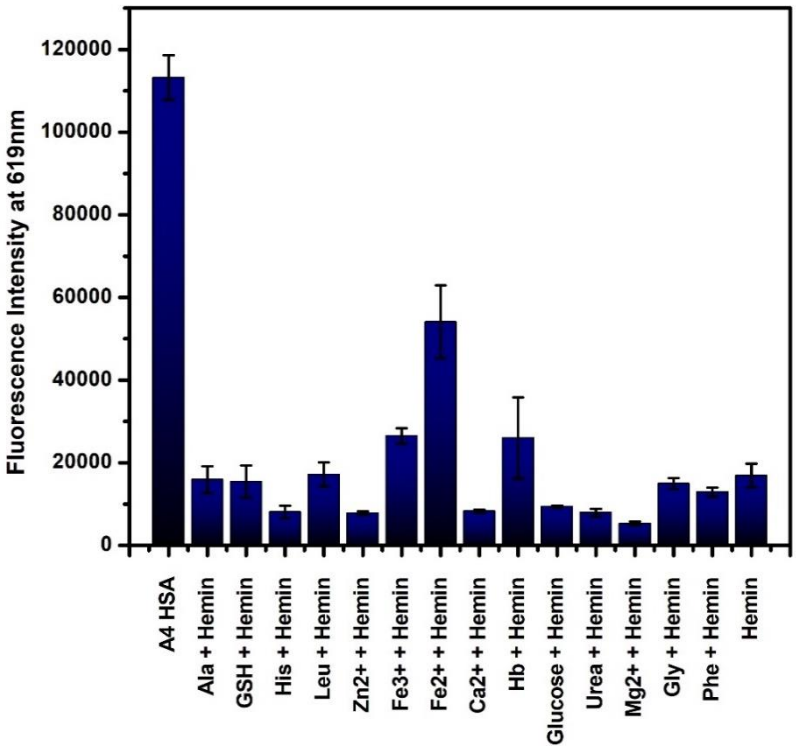

Figure S60: Change in emission intensity of A4- HSA Ensemble upon addition of 100μM of various interferents in PBS in the presence of 10 μM Hemin (pH 7.4).

References:

1. Zayed, M. E. M.; El-Shishtawy, R. M.; Elroby, S. A.; Al-Footy, K. O.; Al-amshany, Z. M., Experimental and theoretical study of donor-π-acceptor compounds based on malononitrile. *Chemistry Central Journal* **2018,** *12* (1), 26.
2. Raftani, M.; Abram, T.; Bennani, N.; Bouachrine, M., Theoretical study of new conjugated compounds with a low bandgap for bulk heterojunction solar cells: DFT and TD-DFT study. *Results in Chemistry* **2020,** *2*, 100040.
3. Shah, K.; Patel, A. L., Synthesis and study of indoloquinoxaline based D-π-A type conjugated molecules as fluorescent probe for hypochlorite detection. *Journal of Molecular Structure* **2024,** *1303*, 137606.
4. Peinado, C.; Salvador, E. F.; Catalina, F.; Lozano, A. E., Solvatochromic and rigidochromic fluorescent probes based on D–π-A diaryl ethylene and butadiene derivatives for UV-curing monitoring. *Polymer* **2001,** *42* (7), 2815-2825.
5. Shen, P.; Hua, J.; Jin, H.; Du, J.; Liu, C.; Yang, W.; Gao, Q.; Luo, H.; Liu, Y.; Yang, C., Recognition and quantification of HSA: A fluorescence probe across α-helices of site I and site II. *Sensors and Actuators B: Chemical* **2017,** *247*, 587-594.
6. Du, J.; Gu, Q.; Chen, J.; Fan, J.; Peng, X., A novel fluorescent probe for the ratiometric recognition of protein based on intramolecular charge transfer. *Sensors and Actuators B: Chemical* **2018,** *265*, 204-210.
7. K. S. M. Salih, *ChemistryOpen* **2022**, *11*, e202100237.
8. P. Makuła, M. Pacia, W. Macyk, *The Journal of Physical Chemistry Letters* **2018**, *9*, 6814-6817.
9. S. Halder, A. K. Pradhan, P. Sivasakthi, P. K. Samanta, C. Chakraborty, *Materials Today Chemistry* **2023**, *32*, 101649.
10. Y. Huang, T. Lv, T. Qin, Z. Xu, L. Wang, B. Liu, *Chemical Communications* **2020**, *56*, 11094-11097.
11. S. Huang, F. Li, C. Liao, B. Zheng, J. Du, D. Xiao, *Talanta* **2017**, *170*, 562-568.
12. J. Fan, W. Sun, Z. Wang, X. Peng, Y. Li, J. Cao, *Chemical Communications* **2014**, *50*, 9573-9576.
13. X. Chao, D. Yao, Y. Qi, C. Yuan, D. Huang, *Analytica Chimica Acta* **2021**, *1188*, 339201.
14. R. Choudhury, S. Rajeshbhai Patel, A. Ghosh, *Journal of Photochemistry and Photobiology A: Chemistry* **2019**, *376*, 100-107.
15. C. Liao, F. Li, S. Huang, B. Zheng, J. Du, D. Xiao, *Biosensors and Bioelectronics* **2016**, *86*, 489-495.
16. Y.-R. Wang, L. Feng, L. Xu, Y. Li, D.-D. Wang, J. Hou, K. Zhou, Q. Jin, G.-B. Ge, J.-N. Cui, L. Yang, *Chemical Communications* **2016**, *52*, 6064-6067.
17. B. Liu, T. Lv, X. Zhao, M. Zhou, C. Song, C. Zeng, T. Qin, Z. Xu, *Spectrochimica Acta Part A: Molecular and Biomolecular Spectroscopy* **2022**, *264*, 120306.
18. Z. Liang, Y. Sun, H. Zeng, K. Sun, R. Yang, Z. Li, K. Zhang, X. Chen, L. Qu, *Analytical Chemistry* **2020**, *92*, 16130-16137.
19. K. Zhu, T. Lv, T. Qin, Y. Huang, L. Wang, B. Liu, *Chemical Communications* **2019**, *55*, 13983-13986.
20. G. Guan, J. Sha, D. Zhu, *Microchemical Journal* **2017**, *133*, 391-397.
21. W. Gao, C. Wang, K. Muzyka, S. A. Kitte, J. Li, W. Zhang, G. Xu, *Analytical Chemistry* **2017**, *89*, 6160-6165.
22. P. Ni, C. Chen, Y. Jiang, Y. Lu, W. Chen, *Sensors and Actuators B: Chemical* **2018**, *273*, 198-203.
23. S. Han, E. Liu, H. Li, *Microchimica Acta* **2005**, *149*, 281-286.
24. Y. Shi, W. T. Huang, H. Q. Luo, N. B. Li, *Chemical Communications* **2011**, *47*, 4676-4678.

25. L. Zhao, F. Chen, W. Huang, H. Bao, Y. Hu, X.-a. Huang, T. Deng, F. Liu, *Sensors and Actuators B: Chemical* **2020**, *304*, 127392.
26. L. Gao, Y. Xiao, Y. Wang, X. Chen, B. Zhou, X. Yang, *Talanta* **2015**, *132*, 215-221.
27. X. Chao, D. Yao, C. Chen, C. Zhang, *Environmental Technology & Innovation* **2023**, *29*, 102969.
28. B. Gogoi, N. S. Sarma, *RSC Advances* **2013**, *3*, 7747-7750.